International Journal of Mechanical Sciences 117 (2016) 115–134

Contents lists available at ScienceDirect

International Journal of Mechanical Sciences

journal homepage: www.elsevier.com/locate/ijmecsci

Compensation for process-dependent effects in the determination of localized necking limits

Junying Min [a,**], Thomas B. Stoughton [b,*], John E. Carsley [b], Jianping Lin [c,**]

[a] Ruhr-University Bochum, Bochum 44780, Germany
[b] General Motors Research & Development, Warren, MI 48095-9055, USA
[c] School of Mechanical Engineering, Tongji University, Shanghai 201804, China

ARTICLE INFO

Article history:
Received 9 May 2016
Received in revised form
8 August 2016
Accepted 12 August 2016
Available online 13 August 2016

Keywords:
Forming limit curve
Nonlinear strain path
Bending effect
Through-thickness stress

ABSTRACT

This work describes a new procedure to remove the differences in measured forming limits obtained from Marciniak and Nakazima tests, which are the two most frequently used testing methods to obtain necking limits for forming limit diagrams (FLD) used in formability analysis of sheet metal stamping processes. The procedure compensates for the combined effects of curvature and nonlinear strain path that occur during these tests, using measurements recorded by digital image correlation (DIC) throughout the deformation history of the point on the test specimen that eventually necks. The severity of forming is then determined by presenting the critical forming conditions in a stress diagram in order to account for the effects of through-thickness pressure that influences the onset of localized necking in the Nakazima test. These stress-based forming limits are then transformed back to the familiar strain limits (or FLD), but now representing the limits under the restriction of in-plane perfectly linear stretching and plane-stress conditions. Accounting for the effects of nonlinear strain path is particularly sensitive to the detection of the actual onset of localized necking, so this work also recommends the use of realistic methods to detect the actual onset of localized necking. The method adopted in this work is based on a new method described by Min et al. [13,14], in which a change in the surface curvature is used to detect a geometric effect associated with the onset of localized necking. In addition to demonstrating that the standard Marciniak and Nakazima tests (punch diameter of 101.6 mm) produce essentially identical limit curves for a 980 MPa grade multi-phase high strength steel after correction for curvature, nonlinear strain path, and pressure, the method is also applied to the analysis of data from a non-standard Nakazima test with a smaller punch diameter of 50.8 mm, where the severity of these processing conditions are significantly enhanced. This additional test is further proof of the validity and comprehensive coverage of the corrections for the different processing conditions involved in measurement of forming limit curves.

1. Introduction

The Forming Limit Diagram (FLD) is an important graphical aid in formability assessment used by the sheet metal forming industry in the analysis of both finite element (FE) simulations of sheet metal forming processes and in physical die tryout. The FLD describes the limit strains, represented by a Forming Limit Curve (FLC) that defines the upper boundary of deformation that sheet metals can endure before the onset of through-thickness or localized necking. This boundary is typically described in a plot of the major principal strain expressed as a function of the minor principal strain. There are two primary tests used to experimentally determine the FLC, developed independently and known as the Nakazima test and the Marciniak test. The Nakazima test [17] uses a hemispherical dome punch, while the Marciniak test [10] uses a cylindrical punch. Both tests involve using a set of several sheet specimen widths with the axisymmetric tool geometries in order to produce a range of straining conditions from uniaxial to equal-biaxial tension. The differences in these two tests, including other variants of test conditions developed from many different academic, government and industrial labs, particularly with respect to the details of the shapes of the specimen geometries, not only affect the resulting strain paths, but also the shape and characteristics of the FLC. These process-dependent differences in forming limits have until now not been adequately addressed in industrial application of the FLD.

Almost since the inception of the FLD, strain paths, sheet

* Corresponding author.
** Co-corresponding authors.
E-mail address: thomas.b.stoughton@gm.com (T.B. Stoughton).

http://dx.doi.org/10.1016/j.ijmecsci.2016.08.008

curvature, and contact pressure have been known to affect necking limits. While the effect of nonlinear strain paths (NLSP) on the necking limit measurement was first experimentally documented by Nakazima et al. [17], little attention was given to a solution to the strain path effect that was reported by Müschenborn and Sonne [16]. The reason for this was primarily because until the mid 1990's, most industrial engineers believed that strain paths were nearly linear in the first draw die, where most of the formability issues arose. Initially there was not much concern about NLSP effects, and few people were even aware of Müschenborn and Sonne's work, or if aware, did not appreciate its importance. Through-thickness pressure also has long been considered to play a significant role in necking. However, pressure effects have not been widely considered in industrial applications of sheet forming processes. The reason for their neglect is attributed to the wide use and acceptance of shell element elements in sheet forming simulations. The through-thickness stress components in shell elements are constrained to remain zero, even in areas of contact between the sheet metal and tool surfaces. The justification of ignoring pressure effects on necking in analysis using shell elements is based on consistency with the justification of using shell elements in the first place, which is that the through-thickness stress components are negligible.

The effect of sheet curvature was more obvious and solutions were adopted very early in industrial practice. The reason for this is that many automotive stampings involve bending sheet metal on sharp features with radii that approach the sheet thickness, so that the strain on the convex side of the sheet shows no sign of necking although it is often well above, sometimes by more than a factor of 2 higher than the FLC in the first draw die. Furthermore, when necks were observed in areas affected by this bending, they were often found in the area where the metal had moved away from the tool contact radius and had flattened out, essentially eliminating the high strain gradient through the thickness. Consequently, most industrial engineers adopted the idea of either restricting the assessment of formability to areas of small curvature, taking advantage of the fact that necking does not occur at sharp radii, or to be more consistent and provide a formability assessment in areas of smaller but nonzero curvature, adopted the intuitively popular idea of comparing the average strain on the mid-plane through the sheet thickness to the FLC. The latter idea became so popular, that when FEA analysis was introduced in the mid-to-late 1990's in commercial analysis codes, the developers adopted the practice of limiting their formability assessments to consider only the membrane values of elements that are subjected to out-of-plane deformation.

The conventional approach to how formability assessment was applied to the analysis of the first draw die process began to unravel as the use of metal forming simulation of stamping processes began to expand in the mid-1990's with the hope to effectively eliminate the high costs of physical die tryout. While consideration of the importance of accounting for NLSPs was essentially restricted to secondary forming processes for most of the following decade, Stoughton [22] emphasized that NLSPs are intrinsic to all forming processes, including the first draw die. Consequently, it was claimed that solutions to the NLSP problem were necessary for all metal forming processes in order to obtain reliable and robust manufacturing solutions. More recently, Leppin et al. [8] showed that a significant portion of the difference in measured forming limits between the Marciniak and Nakazima tests can be removed simply by accounting for NLSP effects in the analysis, which means that NLSP affects not only the use of forming limits, but how the forming limit is defined.

The ability to obtain reliable FLCs, as well as account for NLSP effects, is greatly improved with the use of digital image correlation (DIC) techniques. Several methods [11–14,30,6,9] have been developed to try to either detect the actual onset of localized necking, or define a suitable proxy for the limits based on an engineering approximation for the onset of localized necking in order to avoid the human detection methods from the early development of the FLD. Using DIC, the strain paths of all areas of interest on forming limit test specimens can be tracked precisely, which for the first time, makes it convenient to simultaneously account for effects on the forming process caused by NLSPs. While DIC strain measurements show that the strain paths of Marciniak specimens are nearly linear from zero strain up to the onset of localized necking, significant NLSPs are observed on Nakazima specimens [1,8].

It is important to note that while friction conditions can influence the location of the instability, as well as influence the degree of nonlinearity in the strain path in the area of localization, friction is not expected to have any effect on the necking limit. It can be advantageous to limit frictional influence using lubricants or viscoelastic materials and thus promote localization to occur near the pole of the specimen, but any localization that occurs can provide valid data for an FLD, provided compensation for nonlinear strain path is made. For example, high friction conditions in a Nakazima test might push the eventual instability to occur in the unsupported region of a specimen. In this case, it remains very important to apply the corrections for effects of NLSP and curvature, but not for the pressure effect since in this case there would be no punch contact where the neck occurred.

After compensating the FLC's for the effects of these forming process conditions, they are shown to converge to a single FLC for both tests, corresponding to the FLC for linear strain paths in the absence of through-thickness strain gradients, for in-plane stress conditions in the absence of through-thickness stress, i.e., under plane-stress conditions. The robustness of this experimental correction procedure is demonstrated in a third set of experiments using a 50.8 mm hemispherical dome, which effectively doubles the severity of curvature and pressure conditions that exist with the conventional Nakazima test using a 101.6 mm dome. It will be shown that with the correction procedure, the FLC using the 50.8 mm dome is consistent with the FLC for the 101.6 mm diameter Nakazima and 101.6 mm diameter Marciniak tooling.

2. Effect of processing conditions on localized necking limits

The next three sub-sections respectively review the challenge and solutions for handling effects of NLSP, curvature, and pressure in the use of the FLD. It is assumed that the strain limits for perfectly linear strain paths for in-plane stretching of a particular sheet metal in a process involving no through thickness normal or shear stress are known. The procedure for determining this FLC will be described in a later section. But here, with this FLC for linear in-plane deformation defined, the challenge is to describe the conditions for the onset of localized necking for cases when conditions are different from this simple mode of deformation.

2.1. Nonlinear strain path effects

The fact that NLSPs affect the forming limit strains has been noted by many scholars in the plasticity community, beginning with the seminal work of Nakazima [17]. Among the first to propose a solution to this challenge was Müschenborn and Sonne [16], who devised a method of accounting for the strain path effect based on the work-equivalent plastic strain. Later, Kleemola and Pelkkikangas [7] and Arrieux et al. [2] proposed using a stress-based FLD (or forming limit stress diagram, FLSD), defined with minor and major stresses on the abscissa and ordinate, which for isotropically hardening materials, is equivalent to the solution

proposed by Müschenborn and Sonne [16]. However, all of these authors promoted this solution for application to analysis of secondary forming processes, and since such analyses were relatively rare, awareness of this solution and its true significance did not spread in the engineering community. The importance of NLSPs in the first draw die became evident as automotive manufacturers began to apply simulation with the objective to reduce die tryout costs, leading to an increasing trend to adopt the FLSD or its equivalent to all forming analysis, beginning with Stoughton [22], who demonstrated the value of the FLSD using previously published forming limit data for NLSP of aluminum alloys published by Graf and Hosford [3] and for steel alloys published by other authors.

Stoughton and Zhu [27] demonstrated that if one simply removes the imposed linear strain paths used in the bifurcation analyses by Hill [5] and Stören and Rice [21], these two theoretical models for the conventional strain-based FLD validates the idea of a path-independent FLSD for an isotropically hardening material. Therefore, to the extent that these theoretical models are considered valid, they validate the use of FLSD to provide a solution to account for NLSPs. Although up until then, the determination and validation of the FLSD had been based on calculated stresses from the strain histories using a given material model, Yoshida et al. [31] experimentally demonstrated that the FLSD of an Al–Mg alloy obtained using a servo-controlled, internal pressure, axial load type testing machine is almost path-independent. These results were different from prior studies because the stresses at the onset of localized necking were measured by mechanical relations that did not depend on a material model.

Despite these successes and theoretical arguments that support adoption of the FLSD, large segments of the industry remain reluctant to adopt stress metrics in their formability assessments because it was believed that the low slope of the stress-strain relation would cause stress metrics to loose significant resolution in the determination of the forming severity compared to strain metrics. To address this reluctance, Yoshida et al. [32] recommended an adaptation of the approach originally proposed by Müschenborn and Sonne [16], using instead effective plastic strain (EPS) limits as a function of the ratio of the current principal stresses. Zeng et al. [33] recommended using EPS limits as a function of the ratio of the principal strain rates, after demonstrating that MK Analysis produced the same FLC for nonlinear strain paths when defined in terms of these variables. Stoughton and Yoon [26] recommended a limit on EPS as a function of an angle equal to the arctangent of the ratio of principal strain rates or stresses. In this case the limit is defined by an angle equal to the ratio of the principal strain rates. The resulting polar diagram has characteristics and behaviors similar to those of the conventional strain FLD, and therefore has an additional appeal to those engineers who are already experienced and familiar with the conventional strain FLD. This diagram is called the PEPS Diagram and is already available in some commercial codes. All of these solutions are equivalent to the FLSD for materials that are work hardening isotropically. Variants of solutions to handle NLSP effects continue to be introduced in the literature, including He et al. [4], Volk et al. [29], Nurcheshmeh and Green, [18], Simha et al. [20], Yoshida et al. [32], and Zhu et al. [34].

While most of the focus of NLSP has been directed at the use of FLC data in formability assessment, it obviously plays a role in the interpretation of measurements of the FLC, which in general do not follow linear strain paths. Leppin et al. [8] and Abspoel et al. [1] have already proposed accounting for NLSPs on measurement of forming limits. This idea is extended in this paper to focus on the importance of detecting the actual onset of localized necking, particularly in the analysis of the Nakazima test results, which involve the largest degree of NLSP. As will be explained later, the correction for NLSP is particularly sensitive to the accurate identification of when the start or onset of localized necking occurs during the test. In this paper, we apply the new curvature method for detection of onset of localized necking as described by [13,14]. This method detects a perturbation in a simple curvature fit of the surface along the line that eventually falls into the groove of the neck. The perturbation is obvious because the curvature changes very slowly from frame to frame in the case of the Marciniak test up to the onset of necking instability. There is a similar stability of the curvature in the case of the Nakazima test, after the sheet wraps over the punch. Because the frame to frame variation of the curvature along the direction of the line that eventually necks is slowly varying, a perturbation of the surface associated with onset of necking results in a distinct signal in the frame to frame variation of the fitted curvature. However, other methods of detecting onset of localized necking may be used and combined with the corrections described in this paper.

Finally, in order to extend the corrections to include the contact pressure effects, as will be described later, the method of correction of NLSP used in this paper is necessarily based on stress metrics, which differs from previous correction methods applied to the Nakazima test results.

2.2. Curvature effects

As mentioned in the introduction, the effect of curvature on strains and its impact on determination of conditions for the onset of localized necking was noticed in the early applications of the FLD for formability assessment in die tryout. Most of the industry quickly adopted the intuitive idea that the average strain, i.e., the strain on the middle layer through the sheet thickness, was the appropriate strain metric to use in comparison to the strain FLD. However, to test this assumption, a study of bending under tension was done at General Motors in 1985 by Mark Tharrett. This study was done so that as the use of FLD concepts were extended to simulation analysis, the formability assessments of curved areas of the mesh could be made with more confidence.

Tharrett's experiments involved stretch-forming strips of metal under nearly plane-strain conditions over a set of wedge-shaped punches with different tip radii ranging from 12.5 mm to 0.5 mm. Tharrett also tested five materials including three thicknesses of 1008 AK steel, an Al–Mg–Si–Cu (2000-series) aluminum alloy, and a 70/30 brass alloy. Stretching over these punches produced strain gradients through the sheet thickness that ranged from very low values to values that were initially as high as 200% on initial contact, and remained as high as 70% at the onset of localized necking. Specimens were imprinted on both sides with a 0.5 mm square grid, and strains were accurately measured using a traveling microscope equipped with Vernier calipers. Details of these experiments and results are reported by Tharrett and Stoughton [28] for the three thicknesses of 1008 AK steel. Contrary to expectations, Tharrett discovered that for tests that were stopped just before the onset of localized necking was detectable, the strains on the middle layer were determined to be well above the measured necking limits for in-plane stretching of all five of the metals studied. In fact, the only test specimens where onset of localized necking was detected were those in which the measured strains on the concave side of the sheet were found to be above the necking limit for in-plane stretching. This very surprising result was confirmed in repeated testing of all five metals.

Generally, when necking was observed in specimens, two necks were observed, one on either side of the punch contact area. These two necks were associated with peaks in the major strain. These strain peaks were observed on both the convex and the concave side. However, these two necks were only observed when the measured strain on the concave side on both peaks met or

exceeded the necking limit for in-plane stretching conditions. Although close in value, the magnitude of the two peak strains were generally not equal. This was attributed to imperfect boundary conditions, material inhomogeneity, and some degree of experimental uncertainty in the strain measurement. Although small, these differences were determined to be significant. One specimen was observed to have only a single detectable neck. Although the measured strains on the concave side of this specimen had the typical double peak in the strain distribution, the peak strain on the concave side, on the side of the punch contact that did not show any evidence of necking, was measured to be just below the limit strain for in-plane necking. The measured strain on the other side of the punch, where onset of localized necking was detected, was measured to have a strain just above the necking limit. In order to verify these observations, the judgment as to whether onset of localized necking was observed was independently confirmed by several people. The strain measurements were also repeated and validated by others.

Although this discovery was initially unexpected, in hindsight the experimental observation can be explained by the fact that necking is an instability phenomenon that simultaneously involves the movement of material points at all layers through the sheet thickness. Unlike fracture, which can initiate on one side of a curved surface and propagate through to the other side, the onset of a localized necking instability would require every layer through the sheet thickness to exceed the instability criterion that applies for in-plane stretching. This requirement applies even if the localized necking through a curved section of the sheet is restricted to a wedge of material, where one point of the wedge is on the concave side of the sheet and the other two points on the convex side. In this geometry, one might expect to see evidence of the neck only on the convex side, rather than find evidence of the neck on both sides, as in the case of low curvature. However, this case would still require an instability on all layers because, although the impact to the neck on the concave side goes to zero at the vertex of this wedge, the additional stretch required to accommodate the geometry of the neck on all other layers through the sheet thickness is finite. This explains why localized necking cannot occur in pure bending deformation since the stress on the inner surface remains in compression, i.e. under negative values of stress, and is always below the positive values of the stress limit required to initiate a localized neck.

Stoughton and Yoon [24] extended the interpretation of these experiments, which involved essentially monotonic linear loading under nearly plane-strain tension conditions, to general nonlinear biaxial tensions. Under nonlinear deformation, localized necking is defined to occur on curved sheet metal only when the stresses on all through-thickness layers of the sheet exceed the stress limit that applies under conditions of in-plane stretching. This takes into consideration that in cyclic bending, for example, stresses on a given layer through the sheet may rise above the condition for onset of localized necking, but necking may remain suppressed as long as other layers are simultaneously below the stress limit, even if those layers have been previously above the limit. This concept explains why necking is not an important consideration in incremental forming processes, as discussed by Seong et al. [19], where it is shown that the large strains achieved in incremental forming are the result of a series of multiple local bending/unbending cycles in which one or more layers remain below the threshold for onset of localized necking, even though at other moments during the latter bending/unbending cycle, each layer is exposed to positive stress well above the condition that would permit onset of localized necking.

Consequently, in the experimental determination of the forming limit from the Nakazima test, which has a high curvature, the stresses and strains on all through-thickness layers should be examined to determine the least critical layer, and it is the stress condition on this layer that controls the onset of localized necking instability. In principle, the same consideration is required for the Marciniak test, because, although the punch used has a flat face in the area of the specimen that necks, the bending resistance of the metal usually causes a slight crown to develop that results in through-thickness stress and strain gradients.

2.3. Pressure effects

Through-thickness pressure (negative stress) is widely acknowledged to influence localized necking, but the understanding of this influence is often confused by the lack of distinction between localized necking and fracture, and the physical differences in how these two modes of material failure are affected by non-plane-stress forming conditions. For example, while there may be some more complex behaviors in the fracture limit for plane-stress conditions caused by a Lode angle dependence on fracture, there is almost universal agreement, at least for conditions of a fixed Lode angle, that fracture limits decrease as the mean stress increases. In contrast to this fracture behavior, theoretical considerations lead to the conclusion that mean stress has no effect on localized necking at all.

The basis for this theoretical argument on the effect of mean stress on localized necking was first described by Stoughton and Yoon [25]. It is almost universally accepted that MK Theory, also known as the MK Model, or MK Analysis, developed by Marciniak and Kuczynski [10], is able to predict the onset of localized necking for a given metal described by a set of constitutive equations. In this theory, necking is defined to occur by a numerical algorithm when the strain rate within a defect exceeds the strain rate within the surrounding homogeneous matrix material by a set factor, usually set to a ratio of 10. The defect region is constrained to maintain continuity constraints with the surrounding matrix for a selected strain path imposed on the matrix. The necking limit is defined to be the strain in the matrix at the moment the ratio of strain rates in the defect/matrix exceeds the tolerance. The defect is pre-defined and is most often defined as a small reduction in the initial thickness, but the model has been improved by others to consider other types of inhomogeneity in the material properties, as well as taking into consideration the geometric orientation of the defect. Given that the MK Theory and its improvements are so widely accepted as a realistic model for localized necking instability, they have one thing in common that leads to a very simple answer to the question of the effect of through-thickness stress on the onset of localized necking.

As noted by Stoughton and Yoon [25], one can perform a thought-experiment to answer this question. If one has done an MK analysis to determine the necking limit for a given strain path under plane-stress conditions, what effect would there be if one did the same numerical calculation under a superimposed hydrostatic stress? The answer is simple since plastic strains do not involve plastic dilatancy and therefore the plasticity equations must be insensitive to a superimposed hydrostatic stress, and therefore to the superposition of hydrostatic stress in the MK Analysis, as proposed in the thought-experiment. Although there would be a small effect from the elastic dilatancy, which is removed when the forming forces are removed and the plastic strain limits are determined for the strain path, the constitutive law, which defines the stresses and strains that develop in the matrix and defect, will result in the same strain path and strain rates as were obtained in the MK Analysis under plane-stress conditions. Therefore, the limit strain under superimposed hydrostatic stress would be identical to the limit strains obtained for a given plane-stress condition without the superimposed hydrostatic component. The same logic of the insensitivity of the constitutive model

to a superposition of hydrostatic pressure was also noted to apply to other theoretical models of onset of localized necking, including bifurcation models proposed by Hill [5] and Stören and Rice [21].

Having established by the above arguments that a superimposed hydrostatic stress has no effect on the onset of localized necking, Stoughton and Yoon [25] turned attention to the more important question at hand, which is the effect of σ_3, or through-thickness stress, on the onset of localized necking. They first noted that the conclusion regarding superimposed hydrostatic stress introduces a problem for the original idea of the FLSD, which was motivated to account for NLSP under plane-stress conditions. The problem is as follows: If the FLSD is defined under plane stress conditions as a set of triaxial stress conditions, $(\sigma_1, \sigma_2, 0)$ at the onset of localized necking, then the insensitivity of the onset of localized necking to a superimposed hydrostatic stress (σ_3) means that the following set of non-plane-stress conditions,

$$(\tilde{\sigma}_1, \tilde{\sigma}_2, \tilde{\sigma}_3) = (\sigma_1 + \sigma_3, \sigma_2 + \sigma_3, \sigma_3), \tag{1}$$

will also result in the onset of localized necking. This conclusion applies for any value of $\tilde{\sigma}_3 = \sigma_3$, positive or negative. At first, this result may appear to undermine the value of the approach using stress to deal with NLSP effects, and in fact it does undermine the value of the original proposal based on the FLSD, which remains valid if limited to plane-stress conditions. But the ambiguity of the forming limits under triaxial stress conditions is eliminated by simply subtracting the through-thickness stress, σ_3, from all three principal stresses, leading to the following transformation and equivalent representation,

$$(\tilde{\sigma}_1 - \tilde{\sigma}_3, \tilde{\sigma}_2 - \tilde{\sigma}_3, 0) = (\sigma_1, \sigma_2, 0). \tag{2}$$

As was noted by Stoughton and Yoon [25] this simple transformation removes the ambiguity in the stress limits, which then applies to any triaxial stress condition, and leads to a modification of the original concept of the FLSD by replacing the coordinates of (σ_1, σ_2), which apply under plane-stress conditions, by the "deviatoric" coordinates of $(\sigma_1 - \sigma_3, \sigma_2 - \sigma_3)$, which apply under more general triaxial stress conditions. For convenience, to avoid changing the shape of the stress FLC that applies under plane-stress conditions, it was recommended to subtract σ_3 rather than revise the description of stress limits in terms of the actual deviatoric stresses (by subtracting instead the mean stress from the principal components). Not only is this method a theoretically consistent way to determine onset of localized necking under triaxial stress conditions, but as will be shown in this paper, the transformation enables us to accurately account for and remove the pressure effects from the Nakazima test in the determination of the FLC. This is because in the presence of a negative stress through the sheet thickness, caused by the contact pressure between the sheet and Nakazima punch, will delay the onset of necking, resulting in higher in-plane stresses in order to achieve the localized necking instability condition that applies under plane-stress conditions. Consequently, to identify these equivalent stress conditions that apply under plane-stress conditions, it is necessary to subtract the magnitude of the pressure through the thickness that is associated with the in-plane stresses on each layer of the sheet in the Nakazima test where this pressure is non-zero.

3. Experimental details

The material used for demonstration of the analytical methods was a 1.2 mm thick multi-phase advance high strength steel (AHSS) with a strength class of 980 MPa (MP980), which was composed of ferrite, tempered martensite, and bainite, with the microstructure as shown in Fig. 1. The mechanical properties of the steel at room temperature are listed in Table 1. The following

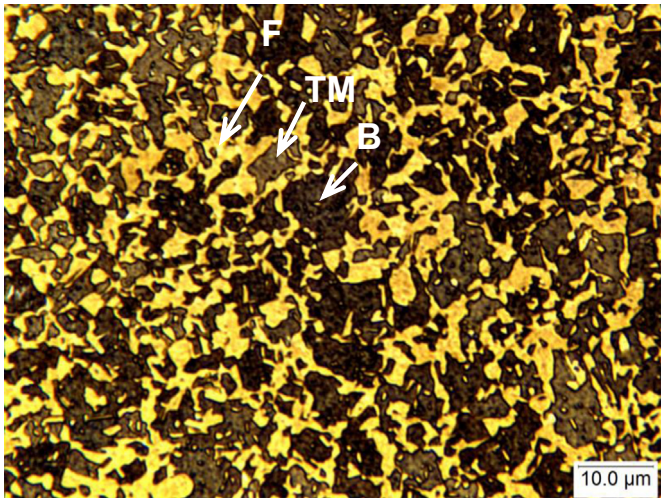

Fig. 1. Optical microstructure of MP980 composed of fine ferrite (F), tempered martensite (TM) and bainite (B). (RD and TD are rolling direction and transverse direction, respectively.).

Table 1
Mechanical properties of MP980. Note: the A, B, C, D and h were fitted from true stress $(\bar{\sigma}_y)$ vs. true plastic strain $(\bar{\varepsilon}_p)$ curve based on the modified Hockett-Sherby hardening law given by Eq. (3).

Lankford coefficients				A	B	C	D	h
0°	45°	90°	$\bar{r}$					
0.84	1.03	1.07	0.99	1122.6	349.15	−7.979	273.57	0.5477

5-parameter modified Hockett-Sherby Law was the best fit to the experimental stress-strain data along the rolling direction of the sheet coil, with the parameters given in Table 1, obtained by least-squares method,

$$\bar{\sigma}_y = A - B\exp\left[-C\left(\bar{\varepsilon}_p\right)^h\right] + D\bar{\varepsilon}_p. \tag{3}$$

where $\bar{\sigma}_y$ is the yield stress, $\bar{\varepsilon}_p$ is the effective plastic strain, A, B, C, h, and D are material constants, obtained by a fit to the stress-plastic-strain data along the RD. The Lankford coefficients, (r_0, r_{45}, r_{90}), are required to calibrate most advanced anisotropic material models. They are also used to calculate the average r value, $\bar{r}$, which is required to calibrate the Hill (1948) Normal Anisotropic Model [35] used in Section 4.2, in Eqs. (11) and (14).

Both Marciniak and Nakazima tests were included in this study. In the Marciniak test, two flat-head punches with a diameter (D_M) of 101.6 mm were used: a conventional Marciniak test with a profile radius (r_M) of 10 mm, and a modified tool with r_M of 25 mm, which was needed to avoid fracture at the profile radius that occurred with some specimen widths for this AHSS. The material of the carrier blank used in the Marciniak test was mild steel with a thickness of 0.7 mm, cut with a central hole diameter of 32 mm. The placement of the specimen and carrier blank in the Marciniak test is illustrated in Fig. 2. In the Nakazima test, two spherical punches with diameters (D_N) of 101.6 mm and 50.8 mm were employed to investigate the effect of bending radius and contact pressure on the forming limits. The non-conventional punch with smaller diameter was employed to amplify the pressure and curvature effects associated with the conventional 101.6 mm Nakazima test for the purpose of putting the analytical methods described in this paper to an extreme test. The tests with 101.6 mm

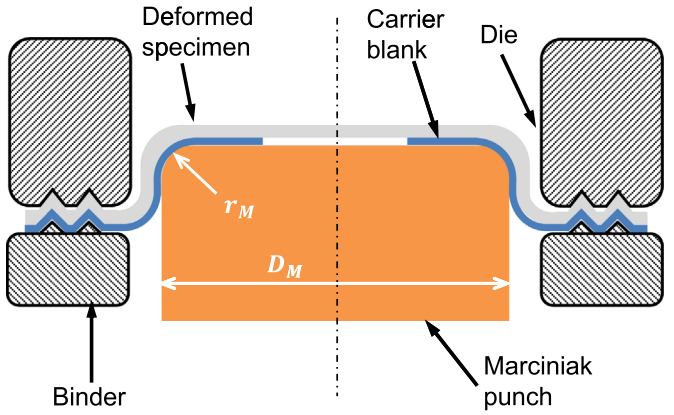

Fig. 2. Illustration of the Marciniak test. Note that two Teflon films (not shown) as lubricant were inserted between the punch and carrier blank, and the conventional deep single-drawbead was modified to shallow double-drawbead to avoid fracture but lock the sheets at binder area during testing.

and 50.8 mm hemispherical punches are designated Nakazima-4 and Nakazima-2, respectively. Thus, three sets of forming limit tests, namely, Marciniak, Nakazima-4 and Nakazima-2 were used to measure three sets of forming limits for the same material in order to confirm the validity of the correction methods and obtain a realistic picture of the actual forming limit of the material under study. The binder and die in all three tests were identical, and the punch stroke rate was set to 0.5 mm/s.

All specimens were rectangular with a length of 180 mm along the rolling direction (RD) of the MP980 sheet. The widths of the specimens were selected following this procedure: firstly, the width of the specimen (w_{FLD0}) associated with plane strain, i.e. minor strain ~0, was determined from a series of tests in all three aforementioned forming limit tests; then 3–4 widths were selected between 20 mm and w_{FLD0} to obtain forming limit data from uniaxial to plane-strain tension and 3–4 widths between w_{FLD0} and 180 mm to obtain forming limit data from plane-strain tension to balanced biaxial stretching. The specimen widths in the three tests are summarized in Table 2.

The applied clamping forces varied from 200 kN to 600 kN for the specimens with widths from 20 mm to 180 mm. No slippage was observed between the binder and each specimen. Furthermore, no specimen fractures occurred in the binder area, which was attributed to the use of shallow double-drawbeads. Two 0.1 mm thick Teflon films with an in-between light layer of grease were inserted between the specimen and the punch for all Nakazima tests or between the carrier blank and the punch in all Marciniak tests to limit the effect of friction.

Digital image correlation (DIC) techniques were applied to measure strains, strain paths, as well as *XYZ*-coordinate data on the outer surface of specimens. To generate the necessary DIC contrast pattern on the outer specimen surface, the following standard procedure was performed: the specimen surface was cleaned with chloroform to remove any oils and dirt; a layer of white paint was sprayed on the cleaned surface followed by a 10 min drying period before applying random speckles of black paint with a size of ~0.5 mm upon the white paint layer. The stereo DIC system included two 4-megapixel cameras, and in all tests, the exposure time and the framing rate of the two cameras were set to 70 μs and 10 frames/s, respectively. The objective in setting the punch speed and frame rate is to ensure that the frame-to-frame strain increments at the time of onset of necking are smaller than the desired precision in the measurement of the strain FLC. Although it is conceivable that one could interpolate a strain limit between two frames, limiting the strain increments makes it convenient to define onset of necking from the data in one frame and directly use the information in this and prior frames to determine the FLC. In the case of the MP 980, at a punch speed of 0.5 mm/s and 10 frames per s, the maximum strain increment from frame-to-frame at the onset of necking was on the order of 0.002. For post-processing of the deformation, an area of interest (AOI) was defined over the center of each specimen, and a grid point spacing with 7 pixels in 29 by 29 overlapping square pixel subsets was set within the VIC-3D 2010 software from Correlated Solutions, Inc.

Here it is worth mentioning that not all specimens listed in Table 2 exhibited localized necking prior to fracture. In particular, the specimens (in either Marciniak, Nakazima-4 or Nakazima-2 test) having strain paths closest to equal-biaxial tension fractured without localized necking, and examples were presented by [13,14], where no change of surface curvature to signal the onset of localized necking was observed in these specimens and cross-sectional views of the fracture also demonstrated the phenomenon, fracture without localized necking. These specimens were summarized in Table 3 and were not included in the following analysis, since fracture limit curve rather than FLC (associated with the onset of localized necking) may be used to assess formability of these specimens. However, the fracture limit criterion is beyond the scope of the current work but will be studied in future.

4. Compensation of the FLC for process-dependent effects

This section describes the procedure to rectify strain measurements at the onset of localized necking in experimental tests, developed to compensate for the effects of curvature (e.g. due to bending), NLSP, and non-zero through-thickness stress (e.g. due to the contact pressure between the tool and sheet specimen) following the ideas described in the previous section. The objective of this compensation is to obtain the FLC for the metal that applies under in-plane plane-stress deformation restricted to perfectly linear strain paths. The validity of this compensation procedure will be demonstrated by showing that the compensated FLC obtained using the Marciniak cylindrical punch is effectively identical to the compensated FLC's obtained using both the Nakazima-2 and Nakazima-4 hemispherical punches.

4.1. Determination of the strain path on all layers through the sheet thickness

As noted in Section 2.2, in order to determine the conditions giving rise to localized necking instability in curved sheet, it is necessary to evaluate the severity of the forming conditions on every layer. However, since the deformation history in both the Nakazima-2 and Nakazima-4 tests, where curvatures are largest,

Table 2
Widths of Marciniak and Nakazima specimens.

Tests	Widths [mm]											
Marciniak	70	90	110	120	128 (w_{FLD0})		135	140	145	150	165	180
Nakazima-4	40	50	60	80	100 (w_{FLD0})	120	135	140	145	150	160	180
Nakazima-2	20	40	50		75 (w_{FLD0})	100	120	140			160	180

Table 3
Summary for fracture and localized necking of Marciniak and Nakazima specimens.

Tests	Punch description	Specimens	Failure locations	Necked or fracture without neck
Marciniak	$D_M = 101.6$ mm, $r_M = 10$ mm	Width $\leq$ 128 mm	Specimen center	Necked
		128 mm < Width $\leq$ 145 mm	Punch profile radius	(Failure in wrong location)
		Width > 145 mm	Specimen center	Fracture without neck
	$D_M = 101.6$ mm, $r_M = 25$ mm	135 mm, 140 mm	Specimen center	Necked
Nakazima-4	$D_N = 101.6$ mm	Width $\leq$ 145 mm	Close to pole	Necked
		Width > 145 mm	Close to pole	Fracture without neck
Nakazima-2	$D_N = 50.8$ mm	Width < 160 mm	Close to pole	Necked
		Width $\geq$ 160 mm	Close to pole	Fracture without neck

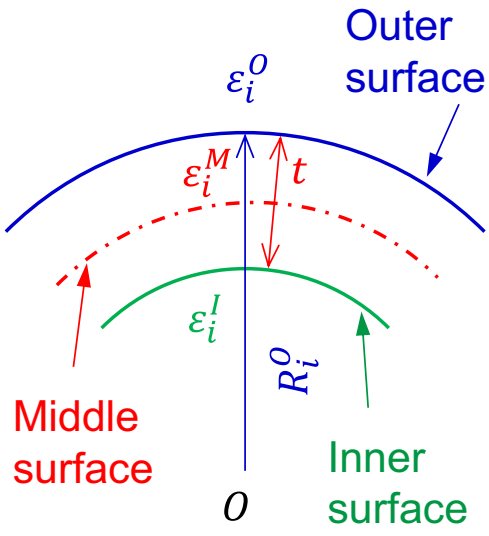

Fig. 3. Illustration for an out-of-plane deformation (i=1, 2 indicate the principal directions).

involves nearly monotonic changes in curvature that at most involve a brief cycle in compression on inner layers, it is considered here to be sufficient to only evaluate the severity of forming on the Outer, Middle, and Inner Surfaces of the sheet, where the "Outer" side refers to the side opposite to the side in contact with the punch. Therefore, it is only necessary to determine the strain history of these three layers. This strain history is defined by three sets of data, $X=(O, M, I)$, respectively representing the strain paths of the Outer, Middle, and Inner Surfaces, symbolically represented by a set of pairs of major and minor principal strains, $\left(\varepsilon_{1,j}^X, \varepsilon_{2,j}^X\right), j=(0, N)$ obtained from N frame images, where the initial strain $\left(\varepsilon_{1,0}^X, \varepsilon_{2,0}^X\right) = (0,0)$. The locations of the three strains on the three surfaces for a given frame image are illustrated in Fig. 3.

The history of the total principal strain on the Outer Surface of the sheet at the point that is identified to be the location where localized necking initiates, is measured directly by the DIC measurement system and extracted for analysis. The entire strain path up to the last DIC frame just before fracture for the Marciniak, Nakazima-4, and Nakazima-2 tests of all specimen widths listed in Table 2 are shown in Fig. 4(a)–(c), respectively. The symbol overlayed on each path in these figures indicate the strain level at the onset of localized necking detected for each specimen.

In conventional analyses of Marciniak and Nakazima tests, without process corrections that are proposed in this work, selecting the correct frame at the onset of necking is important because selection of an earlier (or later) frame, and using the strain level recorded in that frame, would result in lower (or higher) strain limits. This would result in over-estimating (or under-estimating) the possibility of necking in a given metal deformation analysis unless attention was given to ensure that the end frame coincides with the true onset of necking. But the importance of correctly identifying the frame at the onset of necking is even more critical for the compensation required to account for non-linear strain paths. The reason for this higher sensitivity is most easily appreciated by considering the simplistic concept of localized necking, in which the stress state immediately changes to plane-strain stress conditions at the onset of necking. This would be reflected in the DIC data at the point where the increments of minor strain suddenly becomes zero. In this simplistic idea, if the selected frame is even slightly after the onset of necking, then the forming limit would describe a state of plane-strain stress. In this case, one would not obtain a forming limit curve, but a forming limit point, applicable only under plane-strain stress conditions.

Of course the reality is, as seen in Fig. 4, that post necking deformation generally does not immediately change to plane-strain stress conditions, but changes much more gradually. It is clearly seen in this figure that the minor strain increments remain finite between onset of necking and the last recorded frame image. However, the tangents to these strain paths are changing throughout the test, even before reaching the point of necking, but more so after the onset of necking. A change in the direction of the local tangent to these strain paths means that the stress conditions are also changing direction during these tests. While the stress condition generally never reaches plane-strain stress conditions and, since the minor strain increments never go to zero, the process of slowly transitioning towards plane-strain stress conditions after onset of necking moves the critical condition slightly closer to plane-strain stress conditions than is suggested by the value of the net strain. If one selects a frame that is beyond the true onset of necking, it will not only result in an over-estimate of the actual strain limit, but after correction for nonlinear strain path, will end up at a stress condition that is closer to plane-strain stress conditions compared to the stress conditions that existed earlier in the test at the true onset of necking. It is for this reason that it is doubly important to ensure that accurate determination of the onset of necking is employed. In this analysis, onset of localized necking was determined by the curvature method described by [13,14].

Fig. 5 overlays the limit strains determined for all three tests prior to consideration of the effect of the unique processing conditions. While the differences between the Marciniak and Nakazima-4 seem mostly significant on the left hand side of the FLD, which may explain why these differences are often ignored by industry, the superposition of the Nakazima-2 test results clearly show evidence of systematic differences between the hemispherical dome of both Nakazima tests and cylindrical punch of the Marciniak test. These differences can be roughly described as a shift of the entire FLC obtained by the Marciniak test in the direction of a positive increment in the major strain and a positive increment in the minor strains by a magnitude that is roughly proportional to the curvature of the Nakazima punch. The argument that the shift appears to be proportional to the curvature of the Nakazima punch is a consequence of the fact that the location

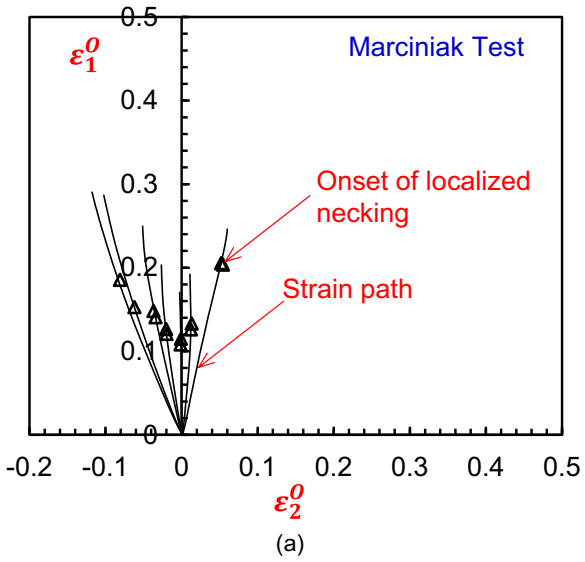

Fig. 4. Strain paths and the limit strains associated with the onset of localized necking in (a) the Marciniak Test, (b) the Nakazima-4 Test and (c) the Nakazima-2 Test. Symbols denote the strain level at which onset of localized necking is detected, which for most strain paths occurs well before fracture of the MP980 steel.

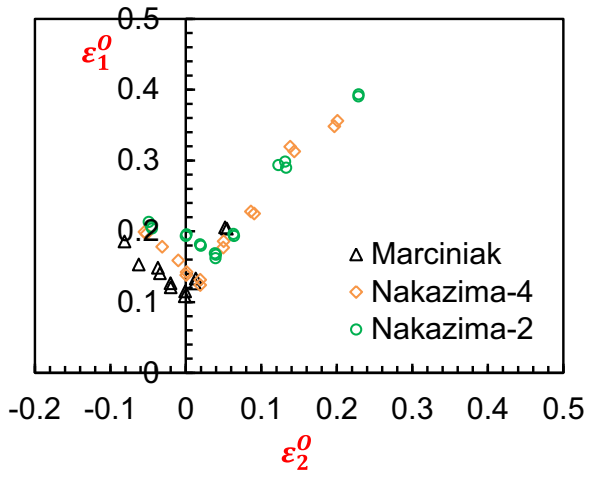

Fig. 5. Comparison of the limit strains from three tests, prior to consideration of the effect of processing conditions those are unique to each test.

of the cusp of the FLC in the case of the Nakazima-2 punch is shifted nearly exactly twice as far from the cusp in the Marciniak test, as the shift of this cusp in the Nakazima-4 test. This shift moves the low point of the FLC from the plane-strain condition to a location with a positive minor strain.

The strain paths on the Middle and Inner Surfaces are a function of the strains on the Outer Surface and the principal curvatures and thickness of the sheet, and therefore require additional calculation effort. As a first step to determine the strains on the other surfaces, it is necessary to determine the curvatures of the sheet on the Outer Surface at the location of the neck. To determine these curvatures, a set of 41 points were extracted from the DIC surface coordinate data through the neck in the direction of the major strain represented by the coordinates, $\left(x_{1,j,k}^O, z_{1,j,k}^O\right) j=(1, N)$, $k=(1{,}41)$. Another set of 41 points were extracted through the localized neck in the direction of the minor strain represented by the coordinates, $\left(x_{2,j,k}^O, z_{2,j,k}^O\right)$, $j=(1, N)$, $k=(1{,}41)$. Sequential points along these perpendicular sections were selected at approximately 0.5 mm intervals in the last DIC frame available, and tracked back through the DIC record to the reference image as material points (where the spacing between these points will be more or less 0.5 mm, depending on whether the section was compressed or stretched in the direction of the corresponding principal strain during the deformation). The 3D surface coordinates, $\vec{x} = \left(x_{1,j,21}^O, x_{2,j,21}^O, z_{1,j,21}^O = z_{2,j,21}^O\right)$ $j=(1, N)$ at the point that is at the intersection of the two sections in all frames, was identified to be the surface coordinate of the point where necking initiated. Once these data sets were extracted, the 2D coordinates of each of the two perpendicular sections, $i=(1{,}2)$, for each frame $j=(1, N)$ were fit to a quadratic equation, $z(x) = a_{i,j} + b_{i,j}x + c_{i,j}x^2$, where $\left(a_{i,j}, b_{i,j}, c_{i,j}\right)$ are the parameters of each fit. Finally the two principal curvatures along the direction of principal strains, $\left(\kappa_{1,j}^O, \kappa_{2,j}^O\right)$ at frame, $j=(1, N)$ were calculated at the intersection of the two sections using the curvature formula for a quadratic curve,

$$\kappa_{i,j}^O = \frac{2c_{i,j}}{\sqrt{b_{i,j}+2c_{i,j}x_{i,j,21}^O}}. \tag{4}$$

The radii of curvatures on the Outer Surface in the directions of the major and minor principal strains $\left(R_{1,j}^O, R_{2,j}^O\right)$ were then defined for each frame, $j=(1, N)$, by inverting the curvatures, $R_{i,j}^O = 1/\kappa_{i,j}^O$.

The fidelity of the quadratic equation $z(x)$ to the DIC data was visually verified during data processing of each test and the calculated curvatures on the Outer Surface was checked for

consistency. For full width specimens, which involve nearly equal-biaxial strain, the two curvatures along the two principal directions were found to be nearly equal. Furthermore, the curvatures were found to be nearly static corresponding to a small crown on the surface of the metal at the location of the neck in the case of the Marciniak test. In contrast, after contact with a punch in the Nakazima tests, a slowly increasing curvature was observed, consistent with the sum of the punch radius and the expected variation of the sheet thickness. In some cases using the narrow width specimens, the calculated curvature along the minor strain direction was noticeably smaller that the major strain axis. This observation is attributed to having insufficient tension in the minor strain direction to overcome the bending resistance of MP 980. Therefore, it is concluded that the above method of curvature determination is sufficiently accurate for this application. However, other algorithms and other parameters of the above algorithm are expected to work just as well in this application. For example, the decision to select 41 points at nominally 0.5 mm spacing was decided primarily to limit file sizes for long term storage of the test results, but have enough points so that the small crown in the Marciniak test was resolved in figures of the DIC data.

The next step for the determination of the strain path on the other layers requires the calculation of the sheet thickness. Since the surface is not flat, both the curvature and strain measurements are factored in the determination of the local sheet thickness. Min et al. [15] derived a cubic equation for calculating the thickness of a stretched curved surface, based on a mapping function described as the "Radius Method" that imposes volume constraints on the deformation described by two principal strains measured on one side of the sheet of an infinitesimal disk mapped onto a curved surface described by two principal curvatures. If t_0 is the initial sheet thickness, $\left(\varepsilon_{1,j}^{O}, \varepsilon_{2,j}^{O}\right)$ are the current principal strains on the Outer Surface, then the sheet thickness t_j at frame $j=(1, N)$ is determined by the following cubic equation,

$$a\cdot t_j^3 - b\cdot t_j^2 + c\cdot t_j - d=0 \tag{5}$$

where

$$a=\exp\left(\varepsilon_{1,j}^{O} - \varepsilon_{2,j}^{O}\right)\cdot\left(R_{2,j}^{O}\right)^2+\exp\left(\varepsilon_{2,j}^{O} - \varepsilon_{1,j}^{O}\right)\cdot\left(R_{1,j}^{O}\right)^2 + \frac{2}{3}R_{1,j}^{O}\cdot R_{2,j}^{O} \tag{6a}$$

$$b = \frac{1}{2}\begin{bmatrix} 2\cdot R_{1,j}^{O}\cdot R_{2,j}^{O}\cdot\left(R_{1,j}^{O} + R_{2,j}^{O}\right) \\ +\exp\left(\varepsilon_{1,j}^{O} - \varepsilon_{2,j}^{O}\right)\cdot\left(R_{2,j}^{O}\right)^2\cdot\left(5R_{1,j}^{O} + R_{2,j}^{O}\right) \\ +\exp\left(\varepsilon_{2,j}^{O} - \varepsilon_{1,j}^{O}\right)\cdot\left(R_{1,j}^{O}\right)^2\cdot\left(5R_{2,j}^{O} + R_{1,j}^{O}\right) \end{bmatrix} \tag{6b}$$

$$c = \frac{1}{16}\begin{bmatrix} 2\cdot R_{1,j}^{O}\cdot R_{2,j}^{O}\cdot\left(5\left(R_{1,j}^{O}\right)^2+5\left(R_{2,j}^{O}\right)^2+6R_{1,j}^{O}\cdot R_{2,j}^{O}\right) \\ +\exp\left(\varepsilon_{1,j}^{O} - \varepsilon_{2,j}^{O}\right)\cdot\left(R_{2,j}^{O}\right)^2\cdot\left(35\left(R_{1,j}^{O}\right)^2+3\left(R_{2,j}^{O}\right)^2+10R_{1,j}^{O}R_{2,j}^{O}\right) \\ +\exp\left(\varepsilon_{2,j}^{O} - \varepsilon_{1,j}^{O}\right)\cdot\left(R_{1,j}^{O}\right)^2\cdot\left(35\left(R_{2,j}^{O}\right)^2+3\left(R_{1,j}^{O}\right)^2+10R_{1,j}^{O}R_{2,j}^{O}\right) \end{bmatrix} \tag{6c}$$

$$d=8\cdot\left(R_{1,j}^{O}\right)^2\cdot\left(R_{2,j}^{O}\right)^2\cdot t_0\cdot\exp\left(\varepsilon_{V,j}^{e} - \varepsilon_{1,j}^{O} - \varepsilon_{2,j}^{O}\right) \tag{6d}$$

and $\varepsilon_{V,j}^{e}$ is the elastic volume change. Note that the parameters, (a, b, c) in Eqs. (5), (6a)–(6c) are unrelated to the $\left(a_{i,j}, b_{i,j}, c_{i,j}\right)$ parameters of the quadratic equation used to calculate the curvatures in Eq. (4). Note also that $\varepsilon_{V,j}^{e}$ is initialized to zero in the calculation of the thickness. Although the neglect of the elastic dilatancy effects is justified in most cases, if greater accuracy in the thickness and stress calculations is desired for high strength steels or light-weighting metals with low elastic moduli, the thickness and stress calculation described later can be updated by iteration using the calculated stresses at each step of the iteration to update the value of $\varepsilon_{V,j}^{e}$ until a converged solution is obtained.

With the thickness, t_j, calculated using the cubic formula in Eq. (5), and the curvatures along the principal strain directions for each frame, the principal strains on the Middle and Inner Surfaces of the sheet specimen are respectively defined by

$$\varepsilon_{i,j}^{M} = \varepsilon_{i,j}^{O} + \ln\left(1-t_j\cdot\kappa_{i,j}^{O}/2\right) \text{ for } i=1, 2, j = (1,N) \tag{7a}$$

and

$$\varepsilon_{i,j}^{I} = \varepsilon_{i,j}^{O} + \ln\left(1-t_j\cdot\kappa_{i,j}^{O}\right) \text{ for } i=1, 2, j = (1,N). \tag{7b}$$

Note that Eqs. (7a) and (7b) can be generalized to calculate the strain history on any specific layer through the sheet thickness, if it was considered necessary to calculate strains on additional layers to find the least critical layer for determination of the conditions controlling the onset of localized necking. This might be important for example, if the location of the neutral axis hops around multiple times, moving from the exterior of one side to the exterior of the other during bending/reverse bending cycles under tension. However, such complex deformation histories do not arise in the Nakazima test, although one compression-tension cycle is observed on the Inner Surface of the sheet in the early stage of deformation.

To illustrate the above strain calculations on the 50 mm wide specimen used in the Nakazima-4 test, Fig. 6 shows the calculated strain paths on the Middle and Inner Surfaces up to the detected onset of localized necking compared to the measured strain path on the Outer Surface. The Outer Surface data corresponds to the strain path shown in its entirety (beyond onset of localized necking) in the second-from-the-left curve shown in Fig. 4(b). As seen in Fig. 6, while the Outer Surface in the Nakazima-4 test first stretches almost equal-biaxially to about 1% strain, the Inner Surface goes into nearly equal-biaxial compression to a similar level of strain, before reversing into tension. The Middle Surface also appears to go into a slightly compressive state, which may be an artifact of a small error in the thickness calculation, or may be caused by the initial deformation required to set the bead or other locking mechanism in the binder while the binder closes. But the dominant initial deformation of the Middle Surface involves stretching in a near plane strain mode (vertical direction) for 2–3%

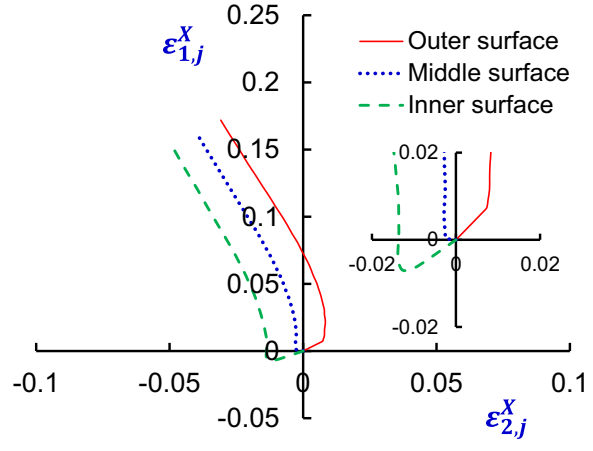

Fig. 6. Strain path ($\varepsilon_{1,j}^{X}$ vs. $\varepsilon_{2,j}^{X}$) on the outer surface, middle surface and inner surface of a 50 mm wide Nakazima-4 specimen.

strain before heading toward a straining direction common to all three layers, which is seen to be midway between plane-strain tension and uniaxial tension. Eventually the strain path on all three layers are observed to follow a parallel path, indicating a common ratio of the principal stresses on all three layers, even though the magnitude of the stress on all layers is expected to be different because of different curvatures and deformation histories.

The final step in preparation for analysis and compensation of the FLC data for NLSP, curvature, and pressure, is to represent the strain history of the three layers, through the sheet thickness, defined by $\left(\varepsilon_{1,j}^{X}, \varepsilon_{2,j}^{X}\right) j=(0, N)$, $X=(O, M, I)$, as a set of N strain increments $\left(\Delta\varepsilon_{1,j}^{X}, \Delta\varepsilon_{2,j}^{X}\right)$, where

$$\Delta\varepsilon_{i,j}^{X} = \varepsilon_{i,j}^{X} - \varepsilon_{i,j-1}^{X} \text{ for } i=1, 2, \text{ and } j=(1,N). \tag{8}$$

4.2. Correction of forming limit for normal anisotropic metals

This section describes the method of correction for a simple model representing metals with normal anisotropy, where the properties through the sheet thickness generally differ from those in the plane of the sheet, while the properties in the plane of the sheet are effectively isotropic. Although the example given will be for a specific model, with additional consideration of minor variants, Section 4.3 describes how to apply this procedure to the most general anisotropic model, and this general case includes the explicit model described in more detail in this section as well as all other "simple" models for in-plane isotropic metals. The more general solution will also enable the correct handling of elastic strains, but for this simple example, we will treat the elastic strains as negligible. However, in order to make this example as accurate as possible, it is necessary to ensure that the total strain increments determined by Eq. (8) are large enough that it makes sense to ignore the elastic contribution within each increment, so that the total strain increments can serve as a proxy for the plastic strain increment. The most convenient way to handle this is to remove data pairs from the data set so that the following requirement is satisfied for successive datums in the $\hat{N}\leq N$ data pairs that remain,

$$\sqrt{\left(\Delta\varepsilon_{1,j}^{X} - \Delta\varepsilon_{1,j-1}^{X}\right)^2 + \left(\Delta\varepsilon_{2,j}^{X} - \Delta\varepsilon_{2,j-1}^{X}\right)^2} \geq \Delta\varepsilon_{min} \text{ for } j=\left(2,\hat{N}\right), \tag{9a}$$

and

$$\sqrt{\left(\Delta\varepsilon_{1,j}^{X}\right)^2 + \left(\Delta\varepsilon_{2,j}^{X}\right)^2} \geq \Delta\varepsilon_{min} \text{ for } j=1. \tag{9b}$$

Because the last strain increment ($j=\hat{N}$) is critical to the correction procedure, this filtering is applied point by point, comparing each data pair to the previous (in time) data pair in the decision to remove the previous data pair and working in the reverse direction down to the first DIC frame. The minimum strain increment, $\Delta\varepsilon_{min}$, is nominally set to 0.01, but the impact of raising or lowering this tolerance by a factor of two was found to be negligible. While a lower bound on the value of $\Delta\varepsilon_{min}$ is essential in the case where the total strains defined by DIC measurements are interpreted as purely plastic strains, it is found that this filtering is not necessary in the more general approach described in Section 4.3, where an elastic model will be used to correctly separate the elastic and plastic components of the total strain. In the simple model covered in this section, however, the $\hat{N}$ plastic strain increments $\Delta p_{i,j}^{X}$ will be assumed to be effectively equal to the $\hat{N}$ total strain increments,

$$\Delta p_{i,j}^{X} \cong \Delta\varepsilon_{i,j}^{X} \text{ for } j=\left(1,\hat{N}\right). \tag{10}$$

This filtering may also be required if the uncertainty in the DIC strain measurement is high, so that a significant component of the strain increments from one frame to the next represent the fluctuation caused by this uncertainty. In this case, the minimum threshold should be at least an order of magnitude larger than the measurement uncertainty. The best approach is to start with small threshold values and increase the threshold until a stable FLC is obtained, but before the threshold for the minimum strain increment is increase so far that the filtered strain path does not track the original DIC recording.

The model chosen to demonstrate the correction method is based on a quadratic, pressure-insensitive yield function with normal anisotropy characterized by a single parameter, $\bar{r}$, known as the normal anisotropy coefficient. The yield function is given by,

$$\bar{\sigma}_y(\sigma_1, \sigma_2) = \sqrt{\sigma_1^2 + \sigma_2^2 - \frac{2\bar{r}}{1+\bar{r}}\sigma_1\sigma_2}. \tag{11}$$

Isotropic hardening is assumed to be characterized by either Swift Law hardening,

$$\bar{\sigma}_y\left(\bar{\varepsilon}_p\right) = K\left(\varepsilon_0 + \bar{\varepsilon}_p\right)^n, \tag{12a}$$

Voce Law hardening,

$$\bar{\sigma}_y\left(\bar{\varepsilon}_p\right) = A - Bexp\left(-C\bar{\varepsilon}_p\right), \tag{12b}$$

or a 5-parameter modified Hockett-Sherby Law (Eq. (3)), where K,ε_0,n, A, B, C, and $\bar{r}$ are material constants. For the MP980 steel used in this study, the modified Hockett-Sherby Law (Eq. (3)) with parameters defined in Table 1 best fit the experimental data. The effective plastic strain is defined by the integral of the effective plastic strain rate, $\dot{\bar{\varepsilon}}_p$

$$\bar{\varepsilon}_p = \int_0^{\tau} \dot{\bar{\varepsilon}}_p d\tau. \tag{13}$$

where τ is the time. The equation for the $\dot{\bar{\varepsilon}}_p$ corresponding to the quadratic yield function given by Eq. (11) is defined in terms of the plastic strain rates, $\left(\dot{p}_1,\dot{p}_2\right)$, as follows

$$\dot{\bar{\varepsilon}}_p\left(\dot{p}_1,\dot{p}_2\right) = \frac{1+\bar{r}}{\sqrt{1+2\bar{r}}}\sqrt{\dot{p}_1^2 + \dot{p}_2^2 + \frac{2\bar{r}}{1+\bar{r}}\dot{p}_1\dot{p}_2} \tag{14}$$

For finite piecewise linear plastic strain increments given by the set of points defined by Eq. (10), the integral in Eq. (13) used to define the total effective plastic strain at the end of the nonlinear strain path on the surface $X=(O, M, I)$ is expressed in terms of the following sum of increments,

$$\bar{\varepsilon}_p^{X} = \sum_{j=1}^{j=\hat{N}} \dot{\bar{\varepsilon}}_p\left(\Delta p_{1,j}^{X}, \Delta p_{2,j}^{X}\right), \tag{15}$$

where $\dot{\bar{\varepsilon}}_p\left(\Delta p_{1,j}^{X}, \Delta p_{2,j}^{X}\right)$ is the 2 parameter function of the strain increments of the form given by Eq. (14), replacing the strain rate variables $\left(\dot{p}_1,\dot{p}_2\right)$ with the strain increment variables $\left(\Delta p_{1,j}^{X}, \Delta p_{2,j}^{X}\right)$.

The next step is to calculate the stress state at the end point of the NLSP. The magnitude of the yield function is obtained simply by substituting the numerical value for $\bar{\varepsilon}_p^{X}$ obtained by solving Eq. (15) into the hardening law (such as Eq. (3), for example). However, to determine the stress condition at the end of forming, we need to employ the flow rule to the yield function (Eq. (11)) to derive the relation between the ratio of the principal stresses, $\alpha=\frac{\sigma_2}{\sigma_1}$, and the ratio of the rate of change of the principal plastic strains $\beta=\frac{\dot{p}_2}{\dot{p}_1}$. For the quadratic yield function, this relation is given by

$$\alpha = \frac{(1+\bar{r})\beta + \bar{r}}{1+\bar{r}+\beta\bar{r}}. \tag{16}$$

Then, the ratio of the principal stresses on the three layers at the onset of localized necking are given by,

$$\alpha^X = \frac{(1+\bar{r})\Delta p^X_{2,\hat{N}} + \bar{r}\Delta p^X_{1,\hat{N}}}{(1+\bar{r})\Delta p^X_{1,\hat{N}} + \bar{r}\Delta p^X_{2,\hat{N}}} \tag{17}$$

where $\left(\Delta p^X_{1,\hat{N}}, \Delta p^X_{2,\hat{N}}\right)$ is the last increment of plastic strain before onset of localized necking, i.e., the last pair of strain increments specified by Eq. (10).

Then, combining Eqs. (3), (11), (15), and (17), the principal stresses at the onset of localized necking along the plastic strain path given by Eq. (10) is

$$\begin{pmatrix}\sigma_1^X\\ \sigma_2^X\end{pmatrix} = \begin{pmatrix}1\\ \alpha^X\end{pmatrix}\frac{\sigma_Y\left(\bar{\varepsilon}_p^X\right)}{\bar{\sigma}_y\left(1,\alpha^X\right)}, \tag{18}$$

where $\bar{\sigma}_y\left(1,\alpha^X\right)$ is the 2-parameter function of the form given by Eq. (11), replacing the principal stresses (σ_1, σ_2) with the following variables $\left(1,\alpha^X\right)$ that represent the relative size of the two principal stresses.

Up to this point, no distinction has been made in the analysis of strain data obtained from the Marciniak, Nakazima-4, and Nakazima-2 tests. In principal, accounting for curvature effects is required in all three tests. This is because there can be a small crown on the sheet deformed by the Marciniak test, depending on material and specimen geometry, that warrants consideration of what is happening on the different layers though the sheet thickness. However, because the crown is so small, the differences in total strain, strain increments, and stresses between the layers for the Marciniak test might be considered negligible. While analysis of the conditions on different layers through the sheet thickness was complete to confirm that the differences in forming conditions on these layers were negligible, for the purpose of this paper, only the strains and stresses on the Outer Surface will be reported for the Marciniak tests to compare to the same calculations on all three layers in the two Nakazima tests.

Fig. 7(a) compares the results of the stress calculations from Eq. (18) on all three surfaces for the Nakazima-4 test to the results of the Outer Surface for the Marciniak test. The data for the three layers in the Nakazima-4 test are distinguished by the symbols associated with labels, N4-O, N4-M, and N4-I. It is noted that the lower bound of these stress conditions on all three layers is calculated to be about 30 MPa higher than the stress limits for the Marciniak test, and this lower bound is observed on the Inner Surface for all specimen widths. Fig. 7(b) shows the same results for the Nakazima-2 test, with the critical stress conditions distinguished by the symbols associated with labels, N2-O, N2-M, and N2-I. In this case, the critical stress conditions are even higher above the Marciniak critical stresses, by nearly 50 MPa for tests closer to equal-biaxial tension, and this lower bound is observed on the Middle Surface of nearly all specimen widths.

Before the cause of these different stress limits is explained, it is helpful to see what the differences mean for strain limits under perfectly linear strain paths. For this purpose, we can calculate the strain limit by assuming a linear strain path to reach the critical stress conditions defined by Eq. (18). The mathematics of this calculation are actually even less complicated than the derivation of Eq. (18), because in calculating the strain limits for linear strain paths, the dependence on the hardening law is removed. The equations defining the strain limits $\left(p_1^X, p_{2,}^X\right)$for a perfectly linear strain path consistent with the stress limit defined by Eq. (18) is

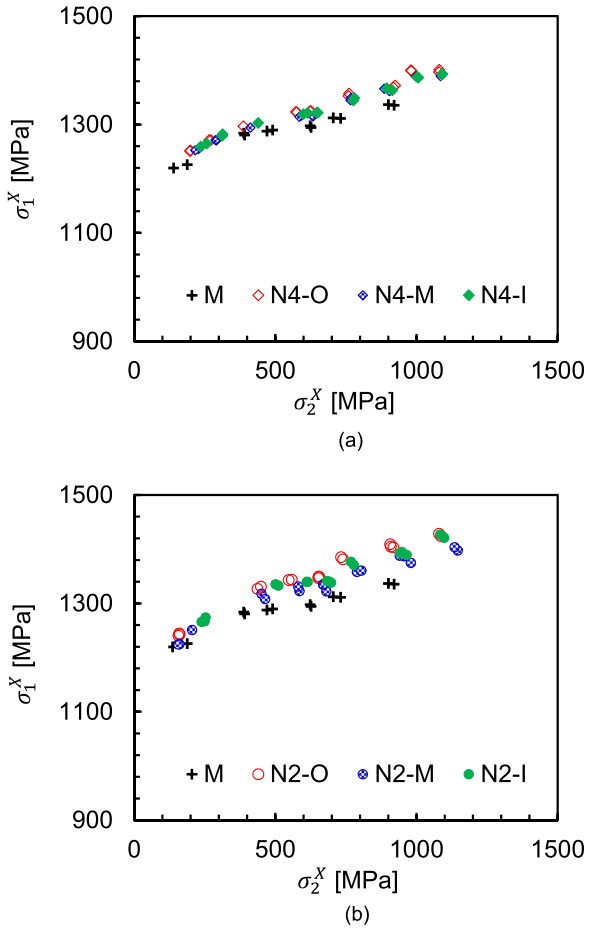

Fig. 7. Stresses calculated on the Outer (O), Middle (M), and Inner (I) surfaces at the onset of localized necking for the (a) Nakazima-4 (N4) and (b) Nakazima-2 (N2) Tests, compared with the stresses calculated for the Marciniak Test (M). The higher limit stresses in the Nakazima Tests compared to the Marciniak Test are expected from the suppression of localized necking caused by the compressive stress through the sheet thickness that exists on the Inner and Middle surfaces of the Nakazima Tests.

given by the following,

$$\begin{pmatrix}p_1^X\\ p_2^X\end{pmatrix} = \begin{pmatrix}\Delta p^X_{1,\hat{N}}\\ \Delta p^X_{2,\hat{N}}\end{pmatrix}\frac{\bar{\varepsilon}_p^X}{\bar{\varepsilon}_p\left(\Delta p^X_{1,\hat{N}}, \Delta p^X_{2,\hat{N}}\right)}. \tag{19}$$

where the numerator on the right hand side is the solution of Eq. (15) and the denominator is the function defined by Eq. (14) evaluated at the last strain increment $\left(\Delta p^X_{1,\hat{N}}, \Delta p^X_{2,\hat{N}}\right)$ leading to the onset of localized necking.

The results of the strain calculations using Eq. (19) are compared in Fig. 8 to the measured (non-corrected) net strains at the onset of localized necking for the a) Marciniak, b) Nakazima-4, and c) Nakazima-2 tests, taking into account NLSP effects, and in the case of the Nakazima tests, also showing the results for the Middle and Inner layers. As noted previously, negligible differences in strain limits were found on the Middle and Inner layers of the Marciniak tests, so only the condition on the Outer layer is shown for the Marciniak test in Fig. 8(a). It may also be noted that there is almost no change to the strain limits for the Marciniak test after correction for NLSP. These results reflect the facts that the radius of curvature of the crown on the surface of the sheet in the area of the neck is more than three orders of magnitude larger than the sheet thickness, and the strain paths in these tests are nearly linear, as seen in Fig. 4(a). On the other hand, the corrections to data

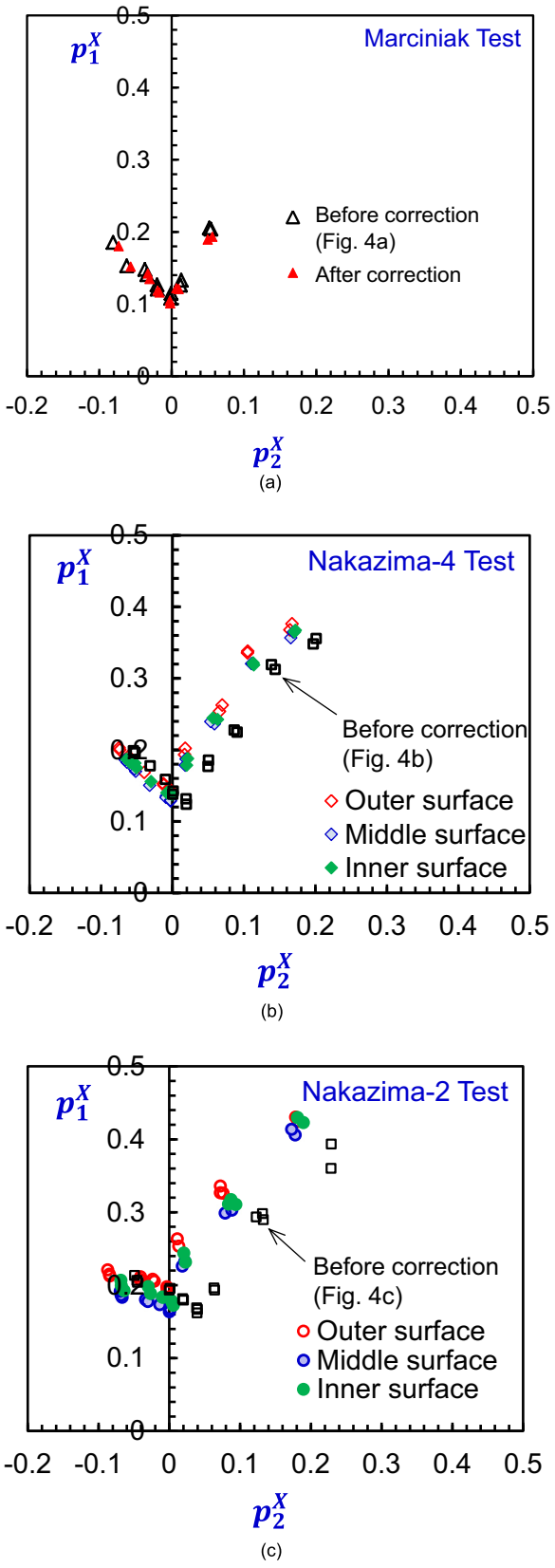

Fig. 8. Comparisons of the limit strains before and after corrections for the effects of curvature and NLSP in (a) the Marciniak Test, (b) the Nakazima-4 Test and (c) the Nakazima-2 Test.

from the two Nakazima tests are significant. As seen in Fig. 8(b), the primary effects of the strain-path corrections to the Nakazima-4 test is to move the minimum in the strain limit for these tests from a small positive value to zero minor strain, and to lower the limit strain on left side in the vertical direction by about 2% strain, and finally to raise the limit strain on the right side of the plane strain stress condition by about 3% strain in the vertical direction. Fig. 8(c) shows the same results for the Nakazima-2 test, where the changes appear to have almost doubled those seen in the Nakazima-4 test. The minimum of the forming limit is moved from an almost doubled positive value to zero minor strain; the lower bound limit strain on the left hand side appears to have been lowered about 4% strain; finally, the strain on the right hand side of plane strain appears to be raised by slightly more than 6%.

Even more enlightening is comparing the lower bound of the path-corrected strain limits on all surfaces of the Nakazima-2 and Nakazima-4, which for these corrections corresponds to the Middle Surface, with the path-corrected limit strains obtained from the Marciniak test. The least critical surface was selected to represent the conditions for the onset of localized necking in the Nakazima tests based on the observations reported in Section 2.2. It is seen in Fig. 9 that the shape of these path-corrected limit strains for all three tests are similar in shape. However, the Nakazima-2 test limit is shifted to significantly higher strain limits than the Marciniak test limits, and the Nakazima-4 test results are midway between these two limits. Despite these different limit strains at this point in the correction procedure, the similarity of the shape suggests a simple explanation and solution to account for and eliminate the remaining differences between these three tests. To account for these differences, it is necessary to return to the representation of the forming limits defined in terms of the stresses.

The final step to determine the stress-based forming limit is to account for the pressure effect using the procedure described in Section 2.3. There is no correction to the stresses calculated by Eq. (18) in the case of the Marciniak test because the area of localized

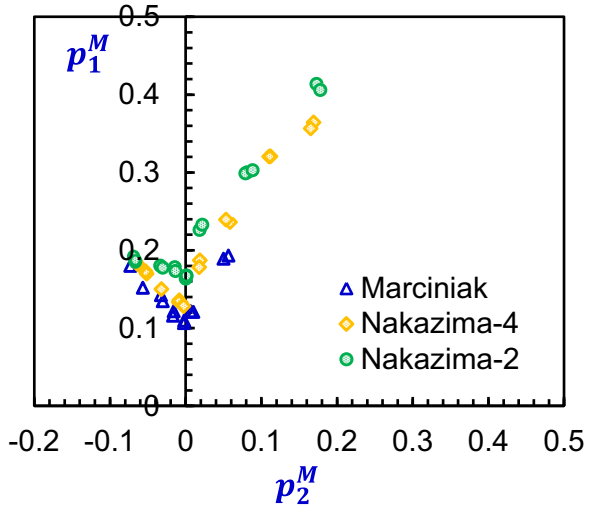

Fig. 9. Strain limits calculated under perfectly linear strain paths to reach the stress limits for the Marciniak Test, and the lower bound strain limits found on the Middle Surfaces of the Nakazima-4 and Nakazima-2 Tests. The equations for these calculations are defined by Eq. (19), which have not yet taken into account the effect of contact pressure. The higher strain limits in the Nakazima Tests are expected from the suppression of necking caused by the through-thickness compressive stress arising from contact with the punch.

necking is not in contact with the punch, so there is no through-thickness pressure effect. There is also no correction to the stresses calculated on the Outer Surface $X=(O)$ for either of the two Nakazima tests because the pressure is zero on this surface. However, there is pressure on the Middle and Inner Surfaces, and as explained in Section 2.3, this compressive stress is expected from necking theory to suppress localized necking in a prescribed way. What this pressure-induced suppression of necking means is that the calculated in-plane principal stresses on these layers will be higher than the principal stress values for localized necking instability under purely in-plane stretching conditions by the magnitude of the pressure on that layer. Representing the contact pressure P as a positive value reflecting a negative through thickness stress on the Inner surface by an amount $\sigma_3 = -P$, the compensated critical stresses on all three layers for the Nakazima test that apply for in-plane stretching conditions are respectively given by,

$$\begin{pmatrix}\sigma_1^O\\ \sigma_2^O\end{pmatrix} = \begin{pmatrix}1\\ \alpha^O\end{pmatrix}\frac{\sigma_Y\left(\bar{\varepsilon}_p^O\right)}{\bar{\sigma}_y\left(1,\alpha^O\right)}, \tag{20a}$$

$$\begin{pmatrix}\sigma_1^M\\ \sigma_2^M\end{pmatrix} = \begin{pmatrix}1\\ \alpha^M\end{pmatrix}\frac{\sigma_Y\left(\bar{\varepsilon}_p^M\right)}{\bar{\sigma}_y\left(1,\alpha^M\right)} - \frac{P}{2}\begin{pmatrix}1\\ 1\end{pmatrix}, \tag{20b}$$

and

$$\begin{pmatrix}\sigma_1^I\\ \sigma_2^I\end{pmatrix} = \begin{pmatrix}1\\ \alpha^I\end{pmatrix}\frac{\sigma_Y\left(\bar{\varepsilon}_p^I\right)}{\bar{\sigma}_y\left(1,\alpha^I\right)} - P\begin{pmatrix}1\\ 1\end{pmatrix}. \tag{20c}$$

The equation for calculating P in the Nakazima test is derived in the Appendix based on the constraints of force equilibrium between the in-plane stresses and the pressure applied on one side of a doubly curved sheet. Note that Eqs. (20a)–(20c) applies for both the Nakazima-4 and Nakazima-2 tests, with the difference being that the pressure P in the Nakazima-2 test is approximately twice as high as the pressure in the Nakazima-4 test. Eqs. (20a)–(20c) also formally applies to the Marciniak test with the understanding that in this case, the pressure P is zero.

Using the formula described in the Appendix to calculate the contact pressure, the compensated stress conditions corresponding to in-plane loading conditions at the onset of localized necking are shown for the Nakazima-4 and Nakazima-2 tests in Fig. 10 (a) and (b), respectively. Note that the Nakazima data for the Outer Surface is unchanged from those test results computed and previously shown in Fig. 7. However, as shown in Fig. 10(a) and (b), the stress limit on the Middle and Inner Surfaces are translated from the stress conditions shown in Fig. 7 in the diagonal direction down and to the left along a vector of length $P_k/\sqrt{2}$ and $\sqrt{2}P_k$, respectively, where P_k is the computed contact pressure at the onset of localized necking for the test specimen k, as computed and tabulated in Table 4. It is seen that the least critical surface in both the Nakazima-4 and Nakazima-2 tests is no longer the Middle Surface, but is now the Inner Surface, where the pressure correction is largest. Based on the discussion in Section 2.2, this is the data that is to be interpreted to represent the critical stress condition of onset of localized necking under plane-stress conditions.

The significance of these compensations is shown in Fig. 11, where for different specimen widths, there is no discernable difference in the stress limits obtained between the Marciniak, Nakazima-4, and Nakazima-2 tests. To have a better handle on the significance of these differences, the stress limits shown in Fig. 11 are converted into corresponding strain limits under the assumption of linear strain path. In this case, Eq. (19) cannot be used because the corrected stress conditions defined by Eqs. (20a)–(20c) include compensations for the pressure. Nevertheless, by inverting Eq. (16) to solve for β,

$$\beta = \frac{(1+\bar{r})\alpha - \bar{r}}{1+\bar{r} - \alpha\bar{r}}. \tag{21}$$

using the ratio of the pressure-corrected principal stresses defined by Eqs. (20a)–(20c) to define the ratio, $\alpha=\sigma_2/\sigma_1$, the following simple equation for this material model applies to the transformation of the stress limit defined by principal stresses (σ_1, σ_2), to a corresponding point on the strain limit for a linear strain path, (p_1, p_2)

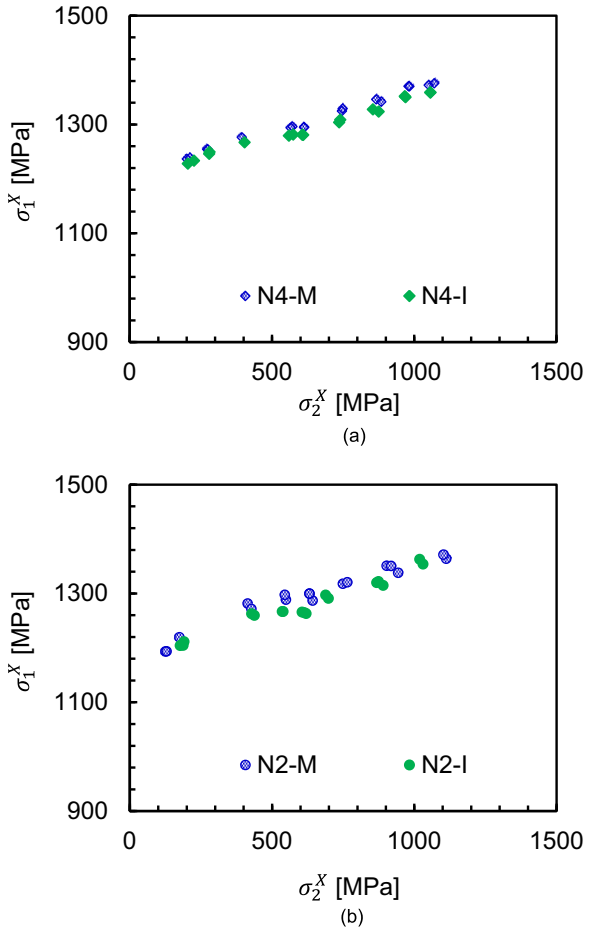

Fig. 10. Stresses (σ_1^X vs. σ_2^X) calculated on Middle (M) and Inner (I) surfaces at the onset of localized necking for the (a) Nakazima-4 (N4) and (b) Nakazima-2 (N2) Tests, after compensation for the through-thickness stress on these surfaces using the data in Table 4.

Table 4
Contact pressure data (P) in the Nakazima tests at the onset of localized necking, based on the calculation procedure detailed in the Appendix.

Nakazima-4	Widths [mm]	40	50	60	80	100	120	135	140	145
specimens	P [MPa]	31.1	32.8	35.8	39.9	40.6	40.2	39.5	36.0	34.1
Nakazima-2	Widths [mm]	20	40	50	75	100	120		140	
specimens	P [MPa]	62.1	73.4	77.2	79.9	79.7	73.9		65.7	

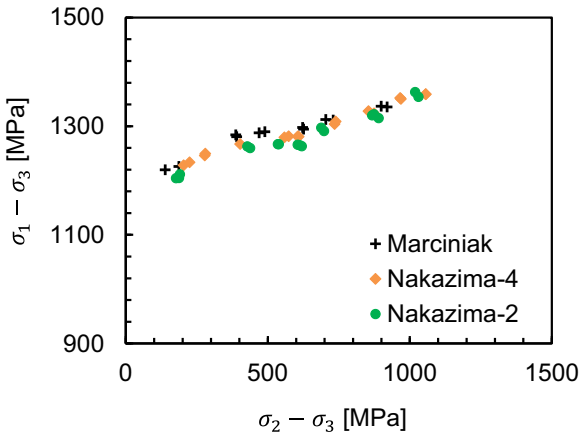

Fig. 11. Consistent forming limits ($\sigma_1 - \sigma_3$ vs. $\sigma_2 - \sigma_3$) from the Marciniak, Nakazima-4 and Nakazima-2 Tests after corrections for the effects of curvature, NLSP and contact pressure.

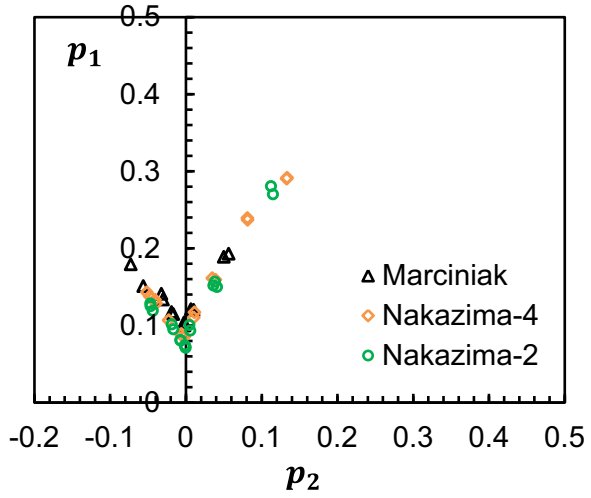

Fig. 12. Forming limits in conventional principal strain space after corrections for the effects of curvature, NLSP, and contact pressure from the Marciniak, Nakazima-4 and Nakazima-2 Tests.

$$\begin{pmatrix} p_1 \\ p_2 \end{pmatrix} = \begin{pmatrix} 1 \\ \beta \end{pmatrix} \frac{\bar{\varepsilon}_p^X}{\dot{\bar{\varepsilon}}_p(1,\beta)}, \tag{22a}$$

where the 2-parameter function $\dot{\bar{\varepsilon}}_p(1,\beta)$ in the denominator is defined by Eq. (14), and the effective plastic strain $\bar{\varepsilon}_p^X$ is obtained by inverting the right hand side of the following relation,

$$\bar{\sigma}_y(\sigma_1, \sigma_2) = \sigma_Y(\bar{\varepsilon}_p) \tag{22b}$$

where the left hand side is defined by Eq. (11), and the right hand side is given by the hardening law selected from the options in Eqs. (12a) and (12b), or in this example, Eq. (3). The results of this transformation are shown in Fig. 12, where it is observed that the compensated strain limits for in-plane linear strain paths obtained from these three tests are now effectively identical.

4.3. Correction of forming limit for anisotropic metals

The compensation procedure for NLSP, curvature, and contact pressure are extended in this section to generally anisotropic metals, including materials with combined isotropic-kinematic hardening, or more generally anisotropic hardening. The analysis will also simultaneously consider both associated and non-associated flow rules, and fully account for elastic strains, even possibly including an anisotropic elasticity model, if desired or necessary. This will all be done without actually going into any further details of the material model. The way this is possible is simply by starting with the fully calibrated "user material model," or UMAT, to process experimental data obtained from DIC measurements under plane-stress conditions for the same metal for which the FLC data is to be processed. The UMAT is used in this application as a standalone code to process the FLC data. Presumably, the material model implemented in the UMAT is the one that best describes the behavior of the metal in question. However, it is recognized that in practice, engineers may need to employ less than the best material model in their FEM simulations of a given metal forming application, perhaps because sufficient data is unavailable to calibrate more accurate models. In this case it is important to note that the procedure described in this work can be applied using any material model that the engineer choses or is restricted to use. While one should expect this choice might introduce errors in the corrections to the FLC, these errors are no more serious than the errors introduced in FEM simulations using these inferior material models.

The material parameters of this UMAT are assumed to be calibrated from material tests, such as hydraulic bulge tests, and uniaxial tension tests along the rolling, transverse, and diagonal directions with respect to the sheet coil, but may also include other tests, such as tension-compression tests, if a kinematic hardening model is required to characterize the material for its intended application. The practical, as well as heuristic, value of starting with this calibrated UMAT, is that it already contains all the mechanical relations required to calculate the change in stress ($\Delta\sigma_{11}, \Delta\sigma_{22}, \Delta\sigma_{12}$) and the decomposition of the total strain increments ($\Delta\varepsilon_{11}, \Delta\varepsilon_{22}, \Delta\varepsilon_{12}$) into increments of the elastic ($\Delta e_{11}, \Delta e_{22}, \Delta e_{12}$) and plastic ($\Delta p_{11}, \Delta p_{22}, \Delta p_{12}$) tensor components. This calculation can be represented symbolically by the following simple functional relationship,

$$\left(\Delta\sigma_{ij}, \Delta p_{ij}, \Delta e_{ij}, \Delta\bar{\varepsilon}_p\right) = \text{UMAT}\left(P_i, \bar{\varepsilon}_p, \sigma_{ij}, \Delta\varepsilon_{ij}\right) \tag{23}$$

where P_i abstractly represents all the parameters of the material model, $\bar{\varepsilon}_p$ is the current effective plastic strain, and σ_{ij} is the current stress tensor. The Δ symbol in front of the other tensor quantities in the output of the UMAT representing the stress and total, elastic, and plastic strain, and the scalar effective plastic strain, denotes the finite increment of these quantities associated with the total strain increment specified in the input of the UMAT. The UMAT is also coded to define the increments to each back-stress tensor component and other state variables, as may be required by the material model, although these are not explicitly referenced in the input and outputs of the UMAT function given above. The point of this representation is, for the purpose of FEA simulation, which is the purpose for which one requires the FLC, all the constitutive equations needed to correct the FLC, for both Marciniak and Nakazima tests, are already defined and available in the same UMAT function that will be used in simulation of deformation processes by FEM analysis.

In the traditional FEM application, the stress and strain tensor increments outputted from the UMAT are integrated to update the stress and strain decompositions in preparation for the next increment in the FEM simulation. But with a few required additional clarifications, this same UMAT may also be employed to process any set of strain increments, including those obtained directly from DIC measurement, and in particular, those representing the strain history up to the onset of localized necking in FLD tests, such as the strain increments defined by Eq. (8). It should be emphasized that some data filtering may be necessary, but only that necessary to minimize the effect of measurement uncertainty in the strain measurement from one frame to the next. The effect of

the measurement uncertainty was eliminated in the previous analysis by ensuring that the strain increments exceeded a threshold defined in Eqs. (9a) and (9b). However, the main reason that tolerance was introduced was to reduce the impact of ignoring the elastic component of the strain. In this more general case, the elastic strain increments will be explicitly calculated and taken into account. Nevertheless, the filtering is recommended to ensure that artificial plastic strain is not introduced by strain measurement uncertainty. This unmistakable sign that measurement uncertainty is affecting the analysis may be determined through inspection of the calculated stress conditions that are determined to be necessary to drive the experimentally measured strain paths. If the calculated stress history in the FLD testing involves repetitive tension-compression cycles, then these can be interpreted to be the result of strain measurement scatter from frame to frame, which can be eliminated using the procedure defined by Eq. (9a) and (9b).

The first clarification in the application of the UMAT for dealing with general anisotropic materials, concerns the fact that like other material behaviors, such as the in-plane variation of the uniaxial tension yield stress or Lankford coefficients (r-values), strain forming limits are generally not isotropic in the plane of the sheet. For example, Graf and Hosford [3] reported significantly different FLCs along the rolling and transverse directions of aluminum alloys. Although it is rarely studied, one would also expect most sheet metals to exhibit differences in necking limits along the direction diagonal to the sheet coil, with as strong anisotropy as is often exhibited in yield stress and Lankford coefficients (r-values) along the diagonal direction compared to the rolling and transverse directions. This issue was avoided in the previous section by using a material model with in-plane isotropy and implicitly using test data for one material orientation as though there was no anisotropy in necking limits.

To handle anisotropic forming limits, Stoughton and Yoon [24] proposed the concept of a forming limit surface constructed from FLC's measured and defined along the rolling (R), diagonal (D), and transverse (T) directions of the sheet. This and other solutions to handle anisotropy in forming limits are most easily implemented from the transformation of DIC measurements of FLD tests with specimens orientated at different angles to the rolling direction using the UMAT approach to data processing. However, in order to account for this anisotropy, a full set of tests must be done along each direction (R,D,T) relative to the sheet coil and analyzed separately. Once this data is collected for one of these directions, and represented in terms of principal strain increments as defined by Eq. (8), these principal strain increments for $j=(1, N)$ must be transformed to tensor components, as follows

$$\Delta\varepsilon^X_{11,j} = \Delta\varepsilon^X_{1,j}\cos^2(\theta) + \Delta\varepsilon^X_{2,j}\sin^2(\theta) \tag{24a}$$

$$\Delta\varepsilon^X_{22,j} = \Delta\varepsilon^X_{1,j}\sin^2(\theta) + \Delta\varepsilon^X_{2,j}\cos^2(\theta) \tag{24b}$$

$$\Delta\varepsilon^X_{12,j}=2\left(\Delta\varepsilon^X_{1,j} - \Delta\varepsilon^X_{2,j}\right)\sin(\theta)\cos(\theta) \tag{24c}$$

where $\theta=(0,45,90)$ for tests along the (R,D,T) directions, respectively. Note that the factor of 2 in Eq. (24c) is introduced to convert that tensor component into a shear strain, which is used in UMAT codes to ensure symmetry of the stiffness matrix. It is interesting to note that the DIC measurement systems actually report strain tensor components so that one could directly calculate these strain tensor components on the Outer Surface of the sheet if the coordinate system was intentionally aligned with the 1-axis parallel to the rolling direction of the sheet. However, using a common alignment of the coordinate system with the material axis complicates the computational effort described in Section 2.1 in the procedure to compute the strain paths in the Middle and Inner Surfaces, which require the principal strain and principal curvature values on the Outer Surface. Consequently, it is more convenient to align the DIC coordinate system with the principal axis of the specimen geometry and to use Eqs. (24a)–(24c) to transform these principal strains to the material coordinate system aligned with the rolling direction of the sheet. However, if the DIC strain tensor components were directly used, one would need to take care to double the $\Delta\varepsilon^X_{12,j}$ values in the calls to the UMAT to account for its use of shear strains.

The second clarification concerns the fact that the UMAT must employ an advanced numerical integration scheme to handle the nonlinearities of the constitutive model and how this deals with finite increments to the total strain tensor input and finite increments of the output variables. This is necessary also in FEM analysis, but approximation schemes are normally introduced in commercial FEM software to efficiently handle analyses with hundreds of thousands of time steps and up to or more than a million elements with as many as 7 integration points. In contrast to the shortcuts required to use a UMAT in FEM analysis, which may require on the order of 10^{12} calls to the UMAT, the number of calls required for complete FLD analysis of up to 7 specimen widths, 500 DIC frames, and 3 orientations for characterization of the necking limit of an anisotropic method is only on the order of 10^4. As a result, it is possible to maintain strict error controls on the UMAT, utilizing high order Runge-Kutta integration schemes that may not be considered practical for FEM simulation, and to ensure precise handling of the elastic-plastic transition, particularly to avoid discontinuities in the constitutive laws that undermine the error control features of the higher order schemes.

The simple procedure for calculating the stress tensor components $\sigma^X_{ij,n}$ and effective plastic strain $\bar{\varepsilon}^X_{p,n}$, for any DIC frame $n=(1, N)$up to the onset of necking at frame N, follows these iterative integrations,

$$\sigma^X_{ij,n} = \sum_{k=1}^{k=n}\Delta\sigma^X_{ij,k}, \tag{25a}$$

and

$$\bar{\varepsilon}^X_{p,n} = \sum_{k=1}^{k=n}\Delta\bar{\varepsilon}^X_{p,k}, \tag{25b}$$

where the increments of the stress tensor components $\Delta\sigma^X_{ij,k}$ and effective plastic strain $\Delta\bar{\varepsilon}^X_{p,k}$ for each frame are calculated from the UMAT as follows:

$$\left(\Delta\sigma^X_{ij,k},\Delta\bar{\varepsilon}^X_{p,k},\ \Delta p^X_{ij,k}\right) = \mathrm{UMAT}\left(P_i,\ \bar{\varepsilon}^X_{p,k-1},\ \sigma^X_{ij,k-1},\ \Delta\varepsilon^X_{ij,k}\right), \tag{25c}$$

and the total strain increments for each frame $\Delta\varepsilon^X_{ij,k}$ are defined from the experimental data as described by Eq. (8) after transforming the strains to a material coordinate system aligned with the rolling direction of the sheet coil. The stress tensor components $\sigma^X_{ij,0}$ and effective plastic strain $\bar{\varepsilon}^X_{p,0}$ used as input to Eq. (25c) for the first DIC frame are initialized to zero. Note also that although Eq. (25c) also calls out the increment of the plastic strain tensor $\Delta p^X_{ij,k}$, the output is not used in the integrations (Eqs. (25a) and (25b)). However, the ability of the UMAT to define the relative magnitude of the plastic strain increment at the onset of necking will be used later in the transformation of the stress limits to strain limits.

At this point in the calculation, the stress tensor components have been calculated for the last frame defined to be the condition at the onset of necking, $\sigma^X_{ij,N}$. To account for the pressure effect in the Nakazima-4 and Nakazima-2 tests, the critical stresses applicable for plane-stress conditions are

$$\begin{pmatrix}\sigma_{11}^{O}\\ \sigma_{22}^{O}\\ \sigma_{12}^{O}\end{pmatrix}=\begin{pmatrix}\sigma_{11,N}^{O}\\ \sigma_{22,N}^{O}\\ \sigma_{12,N}^{O}\end{pmatrix}, \tag{26a}$$

$$\begin{pmatrix}\sigma_{11}^{M}\\ \sigma_{22}^{M}\\ \sigma_{12}^{M}\end{pmatrix}=\begin{pmatrix}\sigma_{11,N}^{M}\\ \sigma_{22,N}^{M}\\ \sigma_{12,N}^{M}\end{pmatrix}-\frac{P}{2}\begin{pmatrix}1\\1\\0\end{pmatrix}, \tag{26b}$$

and

$$\begin{pmatrix}\sigma_{11}^{I}\\ \sigma_{22}^{I}\\ \sigma_{12}^{I}\end{pmatrix}=\begin{pmatrix}\sigma_{11,N}^{I}\\ \sigma_{22,N}^{I}\\ \sigma_{12,N}^{I}\end{pmatrix}-P\begin{pmatrix}1\\1\\0\end{pmatrix}, \tag{26c}$$

where the pressure P is zero for the Marciniak test and also zero for the Nakazima tests in the rare cases when the neck does not occur in the area of contact with the punch. For the more general case in the Nakazima tests, the pressure is calculated from this representation of Eq. (A5) that is derived in the Appendix:

$$P=t\kappa^{I}\left(1+0.5t\kappa^{I}\right)\Sigma \tag{27a}$$

where Σ is the average of the in-plane first invariant of the stress tensor:

$$\Sigma=\frac{1}{4}\left(\sigma_{11,N}^{O}+\sigma_{22,N}^{O}+2\left(\sigma_{11,N}^{M}+\sigma_{22,N}^{M}\right)+\sigma_{11,N}^{I}+\sigma_{22,N}^{I}\right). \tag{27b}$$

The next step is to transform the pressure corrected stress tensor on each layer and convert these back to limits on the plastic strain tensor in the material coordinate system. The equations for this transformation are embedded in the code of the UMAT, but are not directly accessible through the UMAT function to enable such a simple description of the calculation procedure as given by Eqs. (25a)–(25c). A critical component of this transformation is to determine the effective plastic strain $\bar{\varepsilon}_{p,N}^{X}$ associated with the current pressure-corrected stress tensor σ_{ij}^{X} using the following generalization of Eq. (22b) for an anisotropic yield function,

$$\bar{\sigma}_{y}\left(\sigma_{11}^{X},\sigma_{22}^{X},\sigma_{12}^{X}\right)=\sigma_{Y}\left(\bar{\varepsilon}_{p}^{X}\right) \tag{28}$$

Note that if the pressure P is zero, so that $\sigma_{ij}^{X}=\sigma_{ij,N}^{X}$ in Eqs. (26a)–(26c), then the solution for $\bar{\varepsilon}_{p}^{X}$ that solved Eq. (28) is already determined by the integration of Eq. (25b). In other words, $\bar{\varepsilon}_{p}^{X}=\bar{\varepsilon}_{p,N}^{X}$. However, in general, the effective plastic strain for the reduced stresses on the inner layers of the Nakazima tests that satisfies Eq. (28) is less than the effective plastic strain calculated by integrating the increments from the UMAT. In other words, in general, $\bar{\varepsilon}_{p}^{X}\le\bar{\varepsilon}_{p,N}^{X}$.

Eq. (28) can be solved algebraically to determine $\bar{\varepsilon}_{p}^{X}$ for simple hardening laws, such as those given by Eqs. (12a) and (12b), but requires iterative methods if more complex hardening laws are used, such as the Modified Hockett-Sherby law defined by Eq. (3) and used in this study. Once the pressure-corrected plastic strain is determined at the onset of localized necking under plane stress conditions, it can be decided which of the three layers $X\in(O,M,I)$ has the lowest effective plastic strain, to account for the effects of stress and strain gradients through the sheet thickness as discussed in Section 2.2. Let this layer of least plastic work, which defines the critical layer for determination of the onset of localized necking be defined by the symbol $C\in(O,M,I)$, such that the following is satisfied,

$$\bar{\varepsilon}_{p}^{C}=min\left(\bar{\varepsilon}_{p}^{O},\bar{\varepsilon}_{p}^{M},\bar{\varepsilon}_{p}^{I}\right). \tag{29}$$

Note that as discussed in the previous section, for all the Nakazima-4 and Nakazima-2 tests on the MP980 steel, the critical layer was found to be the Inner Surface, $C=I$. Nevertheless, Eq. (29) is recommended to be used for identifying the least critical layer to avoid making any assumption based on experience with limited tests and materials.

Once the critical layer is identified, the plastic strain tensor components for a linear strain path to the stress state defined by the stress tensors components $\left(\sigma_{11}^{C},\sigma_{22}^{C},\sigma_{12}^{C}\right)$ at the onset of localized necking is defined from the plastic flow rule, which can be conveniently defined here

$$p_{ij}^{C}=\bar{\varepsilon}_{p}^{C}\Delta p_{ij,N}^{C}\frac{\bar{\sigma}_{y}\left(\sigma_{11}^{C},\sigma_{22}^{C},\sigma_{12}^{C}\right)}{\sigma_{11}^{C}\Delta p_{11,N}^{C}+\sigma_{22}^{C}\Delta p_{22,N}^{C}+\sigma_{12}^{C}\Delta p_{12,N}^{C}}, \tag{30}$$

where $\Delta p_{ij,N}^{C}$ is the last increment of the plastic strain tensor calculated for the last frame on the critical layer using Eq. (25c). Finally, to convert these plastic strain components into strain limits defined in terms of principal values (presumably these limits are measured along specific directions relative to the sheet coil to account for material anisotropy in the necking limits), the following formula are used, taking into consideration that the p_{12}^{C} component represents the plastic shear strain, and is double the value of the actual tensor component,

$$p_{1}^{C}=\frac{1}{2}\left(p_{11}^{C}+p_{22}^{C}+\sqrt{\left(p_{11}^{C}-p_{22}^{C}\right)^{2}+\left(p_{12}^{C}\right)^{2}}\right) \tag{31a}$$

$$p_{2}^{C}=\frac{1}{2}\left(p_{11}^{C}+p_{22}^{C}-\sqrt{\left(p_{11}^{C}-p_{22}^{C}\right)^{2}+\left(p_{12}^{C}\right)^{2}}\right) \tag{31b}$$

Finally, by following this procedure of calculating the stress limits along the rolling, diagonal, and transverse directions, a forming limit surface can be created following the procedure described by Stoughton and Yoon [24].

5. Discussion

Since the calculated stress FLC in Fig. 11 is dependent on the constitutive model, it cannot be directly applied to the FE analysis when employing a different constitutive model. Material models are often changed in practice as engineers sometimes select simple and less computationally intensive models to obtain results quickly, or select more advanced material models for more accuracy. Therefore, it is of necessity to convert the stress FLC in Fig. 11 back to the conventional strain FLC, defined in principal strain space (as presented in Fig. 12) under the assumptions of linear strain path, in-plane stretching, and plane-stress conditions. To be self-consistent, this conversion back into strain space must use the same constitutive relationships that are used when calculating stress FLC and making the corrections described in this paper. As a result, the FLD in Fig. 12 presents the strain-based forming limits after correcting the issues of curvature, NLSP and contact pressure.

Although results will be slightly different if other constitutive laws are used, as first demonstrated in Stoughton [23], the first order effects of limitations of the constitutive model to account for the actual stress-strain relations are canceled in this conversion back to strain space. To demonstrate this first order cancellation in compensations of the strain limits, the procedure described in Section 4.2 was repeated using the fully anisotropic Hill (1948) model [35] and the Barlat (1989) model [36] with exponent $m=6$, based on experimental r-values. The Barlat 89 model generally has

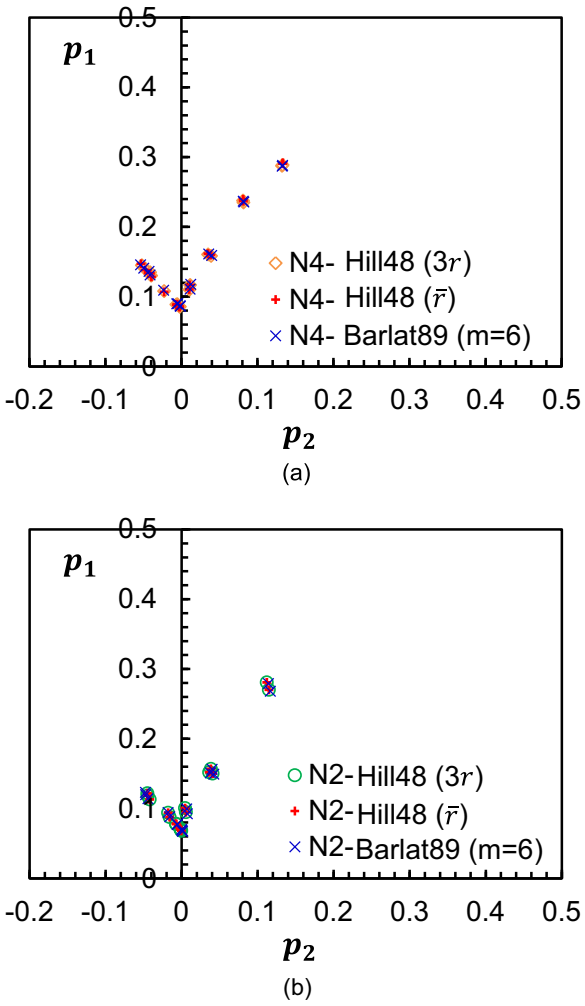

Fig. 13. Comparison of forming limits in conventional principal strain space after corrections for the effects of curvature, NLSP, and contact pressure calculated with three constitutive models from (a) the Nakazima-4 Test and (b) the Nakazima-2 Test.

a lower yield in the plane strain condition and higher yield in the equal biaxial condition, and so is expected to result in a different contribution from the calculated pressures. However, since the pressure corrections are proportional to the calculated stresses, when these stress limits are converted back to strain limits using this same model, there is almost no observed difference in the calculated plastic strain limits, as shown in Fig. 13.

It is also important to emphasize that the FLD shown in Fig. 12 represents only the forming limits for perfectly linear strain paths under in-plane stretching conditions and in the absence of normal through-thickness pressure. When using the FLD in Fig. 12 in a forming simulation that involves even slightly nonlinear strain paths, out-of-plane deformation that leads to sheet curvature, or through-thickness pressure, it is essential to convert this strain limit to a compatible limit criteria that is appropriate to handle these more general forming conditions (e.g. the stress FLD or its equivalent) based on the identical constitutive model that will be employed in the forming simulation. The proof of the necessity of accounting for these three effects in how we use a strain FLC in practice to assess formability where strain paths are even more nonlinear, involve more strongly curved sheet, and higher contact pressures is proven in documenting the effect of these processing conditions between the Marciniak and Nakazima tests, and the ability to correct for these effects so successfully, as shown in Fig. 12.

It is also suggested that the Marciniak test is a better method to obtain forming limit strains, since there are essentially insignificant corrections for the curvature and NLSP effects, and no correction for the contact pressure effect.

While many engineers and scientists are aware of the importance of NLSP on assessment of formability, the fact remains that the strain based FLD is still widely used. It is in fact implemented and treated as a static limit in analysis of complex nonlinear deformation processes in all of the commercial codes, leading to industry-wide error in assessment of formability issues. In the past, one of the justifications for the use of the strain based FLD has been the argument that strain paths in the first draw die are almost linear. And since most of the formability problems occur in the first draw die, it seemed reasonable to ignore these NLSP effects. However, typically on the order of 20% of the metal deformed in the first draw die of automotive stampings are not sufficiently close to being effectively classified as driven along a linear strain path. For example, draw-in from the binder in corner areas, and areas that come into contact with a tool surface late in the forming process to form product features always introduce significant strain path changes, which can either be beneficial or detrimental to the formability in those areas. These things continue to be ignored by large segments in the metal forming industry, resulting in increased costs and lead times when problems occur in tryout. Despite knowing the solution to handle NLSP since the work of Müschenborn and Sonne [16], many engineers continue with the conventional use of the strain base FLD, presumably on the basis that the strain paths in the stamping process that they are responsible for are nearly linear. But the results of this work sheds a new light on this claim. The reason is that most of these engineers would state that the strain paths shown in Fig. 4 are all sufficiently close to linear to be classified as such. And in fact, these strain paths are much more linear that what is typically observed in stamping simulations of actual products. Yet the three tests involved in creating these strain paths result in clearly different necking limits, as seen in Fig. 5. If these small amounts of nonlinearity in these three types of FLD tests lead to such different FLC's, then how can it be justified to ever use the strain based FLD in the way it is widely used today.

In this work, we have shown how to compensate the measurement of the FLC for not only NLSP effects, but also curvature effects, and through-thickness pressure. The implication is that this is only the first part of the story. In order to use this compensated FLC effectively, we must use this knowledge in reverse when we apply it to assess the formability in stamping simulations. This means that the FLC must be represented in terms of metrics that are independent of strain path, which means using stress limits, or its equivalent. In addition, curvature effects must be taken into account by classifying onset of necking in shell elements based on the condition of the least critical integration point through the thickness of the element. The least critical integration point is defined to be the one with the lowest value of the yield function. Finally, for greatest accuracy, it is recommended to use super-shell elements in which the through-thickness stress is calculated from the curvature in equilibrium with the applied in-plane stresses. While such considerations are often widely ignored in industry, the fact that all three of these factors play such a strong role in the interpretation of measurements from the Marciniak and Nakazima tests, emphasizes the importance of these factors in the analysis of actual product manufacturing simulations, where the degree of NLSP, curvatures, and pressure effects are routinely higher by an order of magnitude.

It should also be noted that the final expression of the forming limit given by Eq. (22a) for the example of an in-plane isotropic model and by Eqs. (31a) and (31b) for a more general model, is defined in terms of the plastic strains, rather than the total strain.

This is in accord with the original concept of the FLD for use in die tryout and stamping processes, where strains are measured on parts after removal from the press and reflect the presence of plastic strains after unloading. The same is true for measurement of the FLC's using Circle Grid Analysis, where except in rare cases of processing continuous evolution of strains through images more akin to DIC measurement capabilities, but still using CGA software, experimental strain FLCs also reflect the limits of plastic strain. In contrast to this application, use of the FLD in analysis of FEA results would seem to favor strain limits defined in terms of total strain. In this case, it might seem reasonable to use the total strain as the metric for both the characterization of the FLC and in selecting the FEM results to judge formability. However, as explained in the previous paragraph, in order to account for NLSP in particular, it is necessary to transform the strain limits that apply for perfectly linear strain path into a metric such as stress limits or its equivalent, that account for the dynamic nature of strain limits. With this objective in mind, it does not matter what metric is chosen to represent the strain limits for linear loading, as long as this is taken into account in the conversion to stress limits by the FEM formability analyzer. Consequently, whether the intended application of the strain FLC is for analysis of strains measured on a stamped part, or for analysis of results of FEM simulation, it is sufficient to represent these limits for linear strain paths in terms of the plastic strain.

6. Conclusions and recommendations

Limit major strains associated with the onset of localized necking obtained from the Nakazima tests are higher than those from the Marciniak test, especially on the left hand side of FLD. A smaller punch in the Nakazima test results in even higher limit major strains. Inconsistent limit strains from different forming limit test methods are attributed to the effects of sheet curvature, nonlinear strain path (NLSP), and contact pressure (through-thickness stress) in the area of the neck in the Nakazima tests.

A procedure is developed to correct for the effects of curvature, NLSP, and contact pressure in the three sets of tooling used in this study. After these corrections, all three tests are shown to result in a common limit criterion defined in terms of a stress FLC. Four important conclusions can be drawn from the result that a common limit criterion is obtained for these three tests:

1) The compensation for curvature, NLSP, and contact pressure is correctly handled,
2) No other processing condition that is different between the Marciniak and Nakazima tests plays a role in determining when onset of localized necking will occur, other than through its effect on the strain path of the test,
3) With removal of the strain path effect, there seems to be no reason to require that localized necking occurs at the center of the tool geometry, as long as it occurs within the field of view of the DIC camera system, and
4) In application of the stress limit to general forming conditions, it must be applied in a way such that onset of localized necking is defined to occur ONLY when the stress conditions on all layers through the sheet thickness simultaneously rise above the stress FLC.

The latter conclusion must be implemented in FEM analysis, for example, by requiring the stress conditions at all integration points to be simultaneously above the stress FLC. Because necking requires the simultaneous participation of all layers through the thickness to enable this instability, the implementation of this requirement in formability assessment will explain why localized necking is rarely observed in bending, or in incremental forming processes, where one side tends to cycle into compression or low tension, while the other side simultaneously cycles into tension in the area under deformation.

Forming simulations are most often done using shell elements, where through-thickness stresses are assumed to be zero. The necking limit is uniquely described for use in FEM analysis with shell elements in terms of the in-plane principal stresses. To extend this necking criteria to more general stress conditions, we first consider an extension that introduces only a non-zero through-thickness stress caused by the sheet-to-tool contact pressure, while the through-thickness shear stress components are assumed to remain negligible. This case is considered to be a good approximation in most applications, since prior to the onset of necking, the through-thickness shear stresses arise most commonly from the friction between the sheet and tool. While these through-thickness shear stresses are in fact non-zero when friction is considered, it is true that they are proportional to the pressure by a factor much less than unity in most sheet forming applications. Therefore, it makes sense to consider non-zero normal stress accompanied by zero through-thickness shear stresses before considering the general stress condition, as a first approximation for considering more general triaxial stress conditions. This simplified case is also expected to be the condition of the stress state for the two Nakazima tests, which in the case of the 25 mm radius and 1 mm sheet thickness, involves pressures that are on the order of 4% of the in-plane stress components. Since frictional effects are intentionally minimized in these tests and expected to be an order of magnitude smaller than the contact pressure in typical manufacturing processes, where the friction coefficient is on the order of 0.1, the maximum through-thickness shear stresses would be expected to be on the order of 0.4% of the in-plane stress components.

In the cases where the through-thickness shear stresses are negligible, the principal stresses are aligned with the local normal of the sheet. Two of the principal stresses are in the plane of the sheet, as is the case for plane-stress conditions and shell element analysis. Then, the necking limit is uniquely defined in terms of the “deviatoric” stress diagram using the in-plane components of the principal stress. This extension is most conveniently implemented by subtracting the normal stress from the in-plane principal stresses and using the same stress FLC that applies for plane-stress deformations. Alternatively, a unique stress limit can be obtained by subtracting the mean stress from the two in-plane principal stresses and using the actual in-plane deviatoric stresses as the limits. However, this alternative would change the shape of the stress FLC that is most convenient to use under plane-stress conditions, but leads to equivalent assessments of formability compared to simple subtraction of the normal stress component from the in-plane components.

Although it is out of scope of this application to the analysis of the Nakazima tests, because the through-thickness pressures are relatively small, it is important to consider how to address necking phenomenon under more general triaxial stress conditions, when the through-thickness shear stresses are non-negligible. Unfortunately, there is no experimental data to verify any solution to this more general stress condition. However, for consistency with plane-stress and non-zero normal stress cases, it is reasonable to suppose that necking instabilities would align with the local orientations of the principal stress axes in the general case. In this case, one would expect that if a localized neck would begin to form, it would form in a direction parallel to the three principal stress axes that is most closely aligned with the thickness direction. This is expected because the neck in sheet forming is geometrically constrained to couple the top and bottom surface of the sheet, i.e., the only accessible free edges of the domain of the

metal. In that case, the grooves on the two sides of the sheet would be expected to be displaced from each other in a direction parallel to the plane of the sheet, since in general, the alignment of the principal stresses is not coupled to the surface normal. In any case, this more general treatment is not important in the application of the triaxial stress effects on necking in Nakazima tests because the through-thickness shear stresses are expected to be much smaller than 0.4% of the in-plane stress components.

Although it is recommended to use a material model that best characterizes the deformation of the metal in the compensation for curvature, NLSP, and pressure, it is shown in Fig. 13 that the error introduced in calculating the stress limits using a given material model are canceled to first order when these compensated stress limits are translated back to strain limits for in-plane deformations under conditions of perfectly linear strain paths using the same material model. These "linear" strain limits can then be transformed to stress limits and used for handling "nonlinear" deformations using the best material model appropriate for use in the metal forming simulation, if it is later decided to use for advanced constitutive models. However, it is recommended to always process experimental FLD strain paths data using the most accurate model for the metal that is available, and to redo this analysis when and if more accurate models become available.

Under no conditions is it appropriate to calculate stress FLCs using one material model, and then use this stress FLC to assess the formability in a simulation that uses a different material model.

Using the methods described here, the compensated forming limits obtained from the Marciniak and Nakazima tests are shown to be equivalent, so either test may be used in practice. However, since there is no contact pressure and insignificant contributions from curvature and NLSP effects, the Marciniak test is recommended as the preferred forming limit test method to avoid the calculation uncertainties when applying different constitutive models in the calculation of the limit stresses or estimating and correcting for the contact pressure in the Nakazima test. However, even when the Marciniak test can be used without any corrections, it is nonetheless essential to use it to define the more general forming limit criteria that apply under more general conditions than those of the test, which requires the use of a stress FLC or its equivalent.

Finally, it is necessary to remark on the perception that the Nakazima test is superior because it is better able to populate the right-hand-side of the FLD more completely than the Marciniak test. This perception arises by ignoring the fact that the Nakazima test shifts the necking limit as it occurs under plane-strain stress conditions to a net strain with a positive minor strain, as is seen in Fig. 5. So these tests appear to be telling us something about the forming limits on the right-hand-side of the FLD, but as shown in the corrected results in Fig. 12, these test conditions actually do not describe the forming limit between plane-strain and equal biaxial stress conditions. In fact all of the tests from the Nakazima test are shifted to positive minor strain than is higher than what is compatible with the stress conditions at the onset of necking. Nevertheless, there is a problem with the traditional Marciniak for wider test specimens that are required to probe the metal limits under these biaxial stress conditions.

The problem can be best seen in Fig. 12, that shows the corrected strain forming limits for linear strain paths. As can be inferred from the data in Fig. 4(b), and the information in Tables 2 and 3, the traditional Nakazima test (Nakazima-4) resulted in onset of necking at minor true strains of approximately (+1%, +4%, +8%, and +13%), as observed in Fig. 12, for specimen widths of (120 mm, 135 mm, 140 mm, and 145 mm), respectively. However, as explained in Section 3 and documented in Table 3, these same sample widths resulted in premature fracture at the punch profile radius using the traditional Marciniak test. This premature fracture was caused by bending resistance of MP 980 coupled with frictional effects at the punch profile radius that inhibited further stretching of the specimen about the punch face, and caused localization to occur near the tangent of the punch profile radius. Therefore, a modified Marciniak punch was introduced with the same punch diameter but a much larger profile radius. The punch profile radius was increased to 25 mm, significantly larger than the traditional tool with a profile radius of 10 mm.

As described in Section 3, and documented in Table 3, the 135 mm wide specimen successfully necked using the modified Marciniak punch at the desired location in the center of the specimen. As observed in Fig. 12, this neck is found at a minor strain of slightly more than +5% strain. This is to be compared to the +4% strain realized at the onset of necking using the traditional Nakazima test. Therefore, although the perception may be that the Nakazima test is more capable of characterizing the forming limit for conditions of positive minor strain, here is an example, where by a simple modification of the Marciniak test, we are able to get a comparable if not higher level of minor strain for the same specimen width.

Unfortunately, this modified Marciniak punch did not perform well for wider samples, for which the major strain limit is expected to be higher. In the case of 140 mm and 145 mm wide specimens using the modified Marciniak punch, the hole of the carrier blank had expanded to reach the tangent of the large punch profile radius before the specimen strains reached the necking limit. The edge of this carrier blank under pressure from the punch load carried on the punch profile radius, cause the specimen to prematurely shear. One solution is to reduce the size of the hole in the carrier blank. However, these decreases the effectiveness of the carrier blank, because smaller holes require for energy to expand. A more general solution to this problem is to increase the punch diameter to provide more area for the hole of the carrier blank to expand before reaching the punch profile radius. This solution would require more and larger tooling, perhaps a larger press, and more material for testing, but that would be have to be weighed against the benefits of avoiding the complexity of correcting for contact pressure in the Nakazima test.

Acknowledgments

Junying Min would like to thank the generous support from Alexander von Humboldt Foundation who awarded him a research fellowship at the Ruhr-University Bochum. Junying Min and Jianping Lin would like to acknowledge the financial support for this research provided through the GM collaborative research at Tongji University. The authors would also like to thank the reviewers of the IJMS for their many comments and suggestions to improve the quality of this paper.

Appendix A

Consider an infinitesimal rectangular shell element of thickness t, with principal curvatures, k_1^I and k_2^I on the concave surface (the Inner Surface), and in-plane average stresses σ_1 and σ_2, acting normal to the respective edges of the element along the directions of the two principal curvatures. The force in the direction normal to edge of the element on which the stress σ_1 is applied is,

$$F_1 = \left[\left(R_2^I + t\right)^2 - \left(R_2^I\right)^2\right]\delta\theta_2\sigma_1 \tag{A1a}$$

where $R_2^I=1/k_2^I$ is the radius of curvature of the concave surface of the element in the perpendicular direction, and $\delta\theta_2$ is the infinitesimal half angle of the arc of the edge of the curved element in this direction. The force in the direction normal to the other edge is

$$F_2 = \left[\left(R_1^I + t\right)^2 - \left(R_1^I\right)^2\right]\delta\theta_1\sigma_2 \tag{A1b}$$

where $R_1^I=1/k_1^I$. The component of the force in the direction normal to this element attributed to the above two internal forces, acting on opposing edges of the element, is given by the following sum,

$$F_{int}=4tR_1^I\left(1+0.5t/R_1^I\right)\sigma_2\delta\theta_1\sin(\delta\theta_2)+4tR_2^I\left(1+0.5t/R_2^I\right)\sigma_1\delta\theta_2\sin(\delta\theta_1) \tag{A2}$$

The internal force is assumed to be in equilibrium with the external force arising from an applied pressure P to the concave surface of the infinitesimal element

$$F_{ext}=4R_1^I\sin(\delta\theta_1)R_2^I\sin(\delta\theta_2)P \tag{A3}$$

Equating Eqs. (A2) and (A3), and taking the infinitesimal limits, $\delta\theta_1\to 0$ and $\delta\theta_2\to 0$, results in the following relationship between the principal stresses, curvatures, and pressure:

$$P = t\left[\left(1+0.5tk_2^I\right)\sigma_1k_1^I + \left(1+0.5tk_1^I\right)\sigma_2k_2^I\right] \tag{A4}$$

If $k_1^I = k_2^I = \kappa^I$, the pressure formula simplifies to

$$P = t\kappa^I\left(1+0.5t\kappa^I\right)(\sigma_1+\sigma_2) \tag{A5}$$

As is the case for either the Nakazima-4 test or the Nakazima-2 test in this work, all Nakazima specimens fractured within the contact area between the specimen and the punch; therefore, κ^I is $\frac{1}{50.8}\,\mathrm{mm}^{-1}$ for the Nakazima-4 test and is $\frac{1}{25.4}\,\mathrm{mm}^{-1}$ for the Nakazima-2 test by ignoring the effect of the lubricant (e.g. the 0.1 mm thick Teflon film) between the specimen and punch. However, if a thick lubricant (e.g. ~3 mm or thicker polyurethane sheet) is applied in the Nakazima test, k_1^I may not be equal to k_2^I. Nevertheless, k_1^I and k_2^I can be estimated from the principal curvatures (k_1^O and k_2^O) on the convex surface (the Outer Surface) by Eq. (A6).

$$k_i^I = \frac{k_i^O}{1-tk_i^O}, \quad i=1,2 \tag{A6}$$

References

[1] Abspoel M, Atzema EH, Droog JMM, Khandeparkar T, Scholting ME, Schouten FJ, Vegter H. Inherent influence of strain path in Nakazima FLC testing. In: Guttierez D, (Ed.), Proceedings of the 8th IDDRG Conference, Mumbai. 2011. p. 1–9.

[2] Arrieux R, Bedrin C, Boivin M. Determination of an intrinsic forming limit stress diagram for isotropic metal sheets. In: Proceedings of the 12th biennial congress IDDRG. 1982. 61–71.

[3] Graf AF, Hosford WF. Calculations of forming limit diagrams for changing strain paths. Met Trans A 1993;24:2497–501.

[4] He J, Zeng D, Zhu X, Xia ZC, Li S. Effect of nonlinear strain paths on forming limits under isotropic and anisotropic hardening. Int J Solids Struct 2014;51:402–15.

[5] Hill R. On discontinuous plastic states with special reference to localized necking in thin sheets. J Mech Phys Solids 1952;1:19–30.

[6] Huang G, Sriram S, Yan B. Digital image correlation technique and its application in forming limit curve determination. In: Proceedings of the IDDRG 2008 international conference. Olofstrom, Sweden; 2008, 153–162.

[7] Kleemola HJ, Pelkkikangas MT. Effect of predeformation and strain path on the forming limits of steel, copper and brass. Sheet Met Ind 1977;63 559-591.

[8] Leppin C, Li J, Daniel D. Application of a method to correct the effect of non-proportional strain paths on Nakazima test based forming limit curves. Numisheet 2008;2008:217–21.

[9] Li J, Carsley JE, Stoughton TB, Hector Jr LG, Hu SJ. Forming limit analysis for two-stage forming of 5182-O aluminum sheet with intermediate annealing. Int J Plast 2013;45:21–43.

[10] Marciniak Z, Kuczynski K. Limit strains in the processes of stretch-forming sheet metal. Int J Mech Sci 1967;9:609–20.

[11] Martínez-Donaire AJ, García-Lomas FJ, Vallellano C. New approaches to detect the onset of localised necking in sheets under through-thickness strain gradients. Mater Des 2014;57:135–45.

[12] Merklein M, Kuppert A, Geiger M. Time dependent determination of forming limit diagrams. Ann Cirp 2010;59:295–8.

13 J. Min, T.B. Stoughton, J.E. Carsley, J. Lin. A Method of Detecting the Onset of Localized Necking Based on Surface Geometry Measurements, Submitted for publication.

[14] Min J, Stoughton TB, Carsley JE, Lin J. An Improved Curvature Method of Detecting the Onset of Localized Necking in Marciniak Tests and its Extension to Nakazima Tests, Submitted for publication.

[15] Min J, Stoughton TB, Carsley JE, Carlson BE, Lin JP, Gao XL. Accurate Characterization of biaxial stress-strain response of sheet metal from Bulge testing. Int J Plast 2016. http://dx.doi.org/10.1016/j.ijplas.2016.02.005.

[16] W. Müschenborn, H.M. Sonne. Einfluß des Formänderungsweges auf die Grenzformänderungen des Feinbleches, Arch Eisenhüttenwes 46(1975) 597–602.

[17] Nakazima K, Kikuma T, Hasuka K. Study on the formability of steel sheets. Yawata Tech Rep 1968;264:8517–30.

[18] Nurcheshmeh M, Green DE. Investigation on the strain-path dependency of stress-based forming limit curves. Int J Mater Form 2011;4:25–37.

[19] Seong DY, Haque MZ, Kim JB, Stoughton TB, Yoon JW. Suppression of necking in incremental sheet forming. Int J Solids Struct 2014;51:2840–9.

[20] Simha CH, Inal K, Worswick MJ. Orientation and path dependence of formability in the stress- and the extended stress-based forming limit curves. J Eng Mater Technol 2008;130 041009-1-14.

[21] Stören S, Rice JR. Localized necking in thin sheet. J Mech Phys Solids 1975;23:421–41.

[22] Stoughton TB. A general forming limit criterion for sheet metal forming. Int J Mech Sci 2000;42:1–27.

[23] Stoughton TB. The influence of the material model on the stress-based forming limit criterion. SAE Tech 2002:2002–01-1157.

[24] Stoughton TB, Yoon JW. A new approach for failure criterion for sheet metals. Int J Plast 2011;27:440–59.

[25] Stoughton TB, Yoon JW. Paradigm change: alternate approaches to constitutive and necking models for sheet metal forming. In: AIP conference proceedings 1383. 2011. 15–34.

[26] Stoughton TB, Yoon JW. Path independent forming limits in strain and stress spaces. Int J Solids Struct 2012;49:3616–25.

[27] Stoughton TB, Zhu X. Review of theoretical models of the strain-based FLD and their relevance to the stress-based FLD. Int J Plast 2004;20:1463–86.

[28] Tharrett MR, Stoughton TB. Stretch-bend forming limits of 1008 AK steel. SAE Tech 2003:2003–01-1157.

[29] Volk W, Hoffmann H, Suh J, Kim J. Failure prediction for nonlinear strain paths in sheet metal forming. CIRP Ann Manuf Technol 2012;61:259–62.

[30] Wang K, Carsley JE, He B, Li J, Zhang L. Measuring forming limit strains with digital image correlation analysis. J Mater Process Technol 2014;214:1120–30.

[31] Yoshida K, Kuwabara T, Narihara K, Takahashi S. Experimental verification of the path-independence of forming limit stresses. Int J Form Process 2005;8:283–98.

[32] Yoshida K, Kuwabara T, Kuroda M. Path-dependence of the forming limit stresses in a sheet metal. Int J Plast 2007;23:361–84.

[33] Zeng D, Chappuis L, Xia ZC, Zhu X. A path independent forming limit criterion for sheet metal forming simulations. SAE Tech Pap 2008 10.4271/2008-01-1445.

[34] Zhu X, Chappuis L, Xia ZC. A path-independent forming limit criterion for stamping simulations. In: AIP conference proceedings 778. 2005. p. 459.

[35] R. Hill. The Mathematical Theory of Plasticity, Oxford University Press, 50–58.

[36] F. Barlat, J. Lian. Plastic behavior and stretchability of sheet metals. Part I: A yield function for orthotropic sheets under plane stress conditions, Int. J. of Plasticity, 5, 51–66.